AGU PUBLICATIONS

JGR

Journal of Geophysical Research: Oceans

RESEARCH ARTICLE

10.1002/2016JC011699

Synoptic forcing of wind relaxations at Pt. Conception, California

Melanie R. Fewings[1], Libe Washburn[2], Clive E. Dorman[3], Christopher Gotschalk[2], and Kelly Lombardo[4]

[1]Department of Marine Sciences, University of Connecticut, Groton, Connecticut, USA, [2]Marine Science Institute and Department of Geography, University of California, Santa Barbara, California, USA, [3]Scripps Institution of Oceanography, University of California, San Diego, California, USA, [4]Department of Marine Sciences, University of Connecticut, Groton, Connecticut, USA

Key Points:
- The wind relaxes, enabling poleward ocean flow, due to offshore extension of the desert heat low
- This happens after the North Pacific High extends northeastward as part of a known event cycle
- Offshore extent of relaxation is ~600 km, same as California-scale expansion fan and prevailing wind

Correspondence to:
M. Fewings,
melanie.fewings@uconn.edu

Citation:
Fewings, M. R., L. Washburn, C. E. Dorman, C. Gotschalk, and K. Lombardo (2016), Synoptic forcing of wind relaxations at Pt. Conception, California, *J. Geophys. Res. Oceans*, *121*, 5711–5730, doi:10.1002/2016JC011699.

Received 4 FEB 2016
Accepted 8 JUL 2016
Accepted article online 14 JUL 2016
Published online 11 AUG 2016

Abstract Over the California Current upwelling system in summer, the prevailing upwelling-favorable winds episodically weaken (relax) or reverse direction for a few days. Near Pt. Conception, California, the wind usually does not reverse, but wind relaxation allows poleward oceanic coastal flow with ecological consequences. To determine the offshore extent and synoptic forcing of these wind relaxations, we formed composite averages of wind stress from the QuikSCAT satellite and atmospheric pressure from the North American Regional Reanalysis (NARR) using 67 wind relaxations during summer 2000–2009. Wind relaxations at Pt. Conception are the third stage of an event sequence that repeatedly affects the west coast of North America in summer. First, 5–7 days before the wind weakens near Pt. Conception, the wind weakens or reverses off Oregon and northern California. Second, the upwelling-favorable wind intensifies along central California. Third, the wind relaxes at Pt. Conception, and the area of weakened winds extends poleward to northern California over 3–5 days. The NARR underestimates the wind stress within ~200 km of coastal capes by a factor of 2. Wind relaxations at Pt. Conception are caused by offshore extension of the desert heat low. This synoptic forcing is related to event cycles that cause wind reversal as in Halliwell and Allen (1987) and Mass and Bond (1996), but includes weaker events. The wind relaxations extend ~600 km offshore, similarly to the California-scale hydraulic expansion fan shaping the prevailing winds, and ~1000 km alongshore, limited by an opposing pressure gradient force at Cape Mendocino.

1. Introduction

1.1. The California Current Upwelling System and Wind Relaxations

In summer, the prevailing winds off the west coast of North America are upwelling-favorable (Figure 1). Along the West Coast, the oceanic California Current flows equatorward [*Hickey*, 1979; *Lynn and Simpson*, 1987]. As the water moves equatorward, wind-driven coastal upwelling brings cold water to the surface. This upwelling has both positive and negative effects on the California Current large marine ecosystem. The upwelled water is nutrient-rich and supports high primary productivity and fisheries productivity [e.g., *Pauly and Christensen*, 1995]. However, the upwelled water can also be oxygen-poor and low in pH. Hypoxic, acidic upwelled water contributes to the die-offs of fish and invertebrates that have been a major problem off Oregon in recent years [*Grantham et al*., 2004; *Chan et al*., 2008].

The prevailing upwelling-favorable winds episodically weaken ("relax") for several days and occasionally reverse direction. These wind relaxations reduce nutrients supplied by upwelling, but may also alleviate the corrosive effects of upwelling. Near Pt. Conception at the border between central and southern California (Figure 1), the wind weakens every ~10 days [*Melton et al*., 2009]. These relaxations allow anomalously warm water to move poleward within ~50 km of the coast, both within the Santa Barbara Channel [e.g., *Harms and Winant*, 1998] and poleward of Pt. Conception along central California [e.g., *Washburn et al*., 2011], counter to the prevailing California Current. These buoyant coastal flows change the water temperature along central California and appear to transport larvae from southern to central California [personal communication, E. A. Hoaglund]. For these reasons, it is important to understand what causes wind relaxations near Pt. Conception.

© 2016. American Geophysical Union. All Rights Reserved.

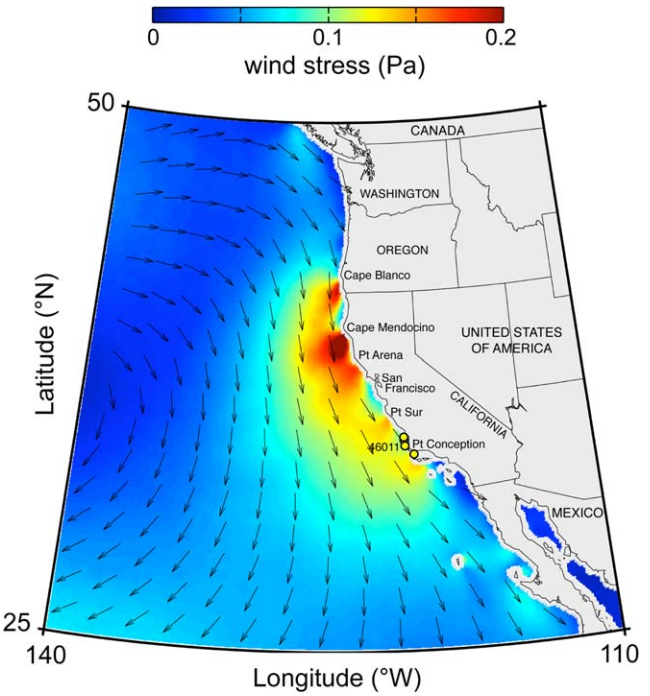

Figure 1. Mean wind stress at sea level during May–August 2000–2009 from QuikSCAT satellite. Color indicates wind stress magnitude and arrows indicate wind stress direction. Arrows are subsampled. The maximum wind stress is 0.26 Pa, though the color scale is cut off at 0.2 Pa. Grey area near land indicates no data where the satellite footprint overlaps land or <10 satellite passes were available for morning or evening. The enhanced wind stress over the California Current upwelling region is visible as a large red-yellow area. Surface wind measurement locations at NDBC buoys 46011, 46023, 46062, and 46054 are indicated by yellow circles near Pt. Conception; only 3 of the 4 circles are visible.

1.2. Prevailing Winds Over the California Current System

The prevailing equatorward winds are intensified within ~400 km of the coast (speeds >8 m s^{-1}) [*Nelson and Husby*, 1983]. The wind is further intensified downstream of the 5 major coastal capes. This wind pattern is due to 8 factors as described below: (1) the North Pacific High (NPH) and (2) low pressure over the southwest United States (U.S.), (3) an air temperature inversion and associated strong vertical gradient in air density, (4) an atmospheric marine boundary layer (MBL), (5) oceanic upwelling, (6) a meridional coastline with coastal mountains parallel to the coast, (7) major capes, and (8) hydraulic MBL dynamics.

The primary factors driving the prevailing wind pattern are the NPH and the desert heat low [*Halliwell and Allen*, 1987]. The NPH is an atmospheric pressure system with mean summer position centered near 40°N, 135°W, ~2000–3000 km west of California [*U.S. Navy*, 1956]. It drives an anticyclonic wind pattern with equatorward winds along the west coast of the U.S. [*Nelson*, 1977]. Heat-generated low-pressure areas over the southwest U.S. combine with the NPH to intensify the equatorward winds [*Halliwell and Allen*, 1987] and generate sea-level pressure isobars parallel to the coast offshore but crossing the coast at an angle along northern California (e.g., Figure 2c). Air moving around the northeast side of the NPH subsides, warming adiabatically and causing a ~500–800 m thick air temperature inversion and associated layer of strong density stratification [*Neiburger et al.*, 1961] that is lowest and strongest at the coast [*Dorman et al.*, 2000]. That density stratification sets the upper limit of the MBL.

The MBL is a moist, cool atmospheric layer between the hot, dry base of the air temperature inversion and the sea surface under the NPH [*Neiburger et al.*, 1961]. The MBL has a bulk temperature similar to the local sea-surface temperature (SST). Wind-driven coastal upwelling decreases the SST near the coast, increasing the density contrast between the air above the inversion and in the MBL. The mean MBL tilts downward toward the east, with the thinnest MBL, ~200 m thick from the sea surface to the base of the air temperature inversion, over the coast between Cape Mendocino and Point Conception [*Dorman et al.*, 2000]. At the top of the MBL is a wind jet [*Zemba and Friehe*, 1987]. Equatorward of Point Conception in the Southern California Bight, the cross-coast trend in MBL thickness is reversed so that the thickness doubles at the coast compared to offshore [*Dorman and Winant*, 1995; *Dorman and Koračin*, 2008].

The coastal mountains are higher than the mean MBL depth along all of California [e.g., *Beardsley et al.*, 1987] and limit cross-shore winds in the MBL everywhere north of Point Conception, except at the gap in the coastline at San Francisco (Figure 1). The winds near the coast tend to be oriented parallel to the coast, partly due to blocking of cross-coast winds by the coastal mountains. Also, the isobars between the NPH and desert heat low are nearly parallel to the coast off central California, so winds in the frictional marine boundary layer will be nearly aligned with the coast [*Halliwell and Allen*, 1987]. The result is that marine air within ~100 km of the coast flows parallel to the local coast and along the along-coast pressure gradient

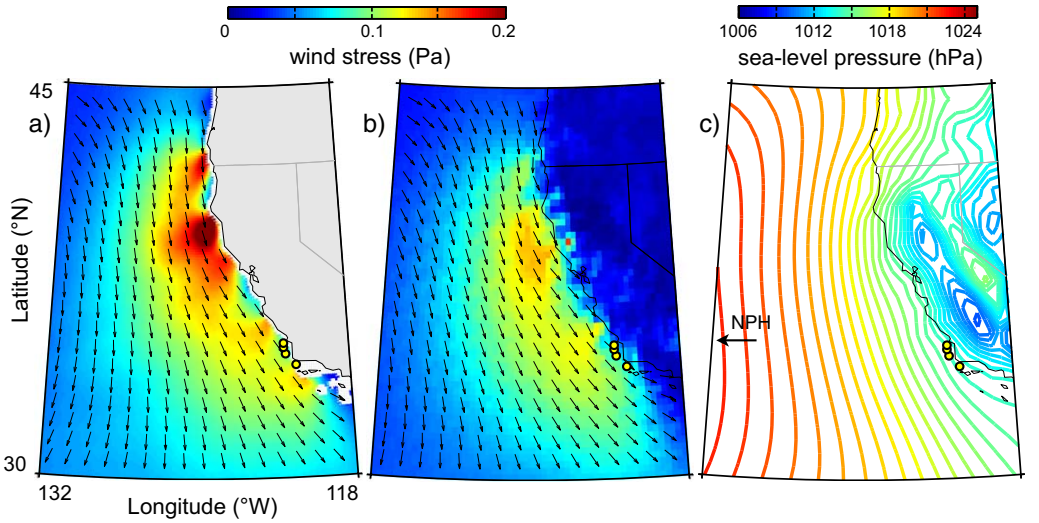

Figure 2. Mean wind stress and atmospheric pressure during May–August 2000–2009. (a) Mean wind stress from QuikSCAT satellite, as in Figure 1; color indicates wind stress magnitude and arrows indicate wind stress direction. Arrows are subsampled. (b) Wind stress, similar to (a) but from the reanalysis NARR at sea level. (c) Atmospheric pressure at sea level from NARR. NPH indicates the direction to the center of the North Pacific High. The contour interval is 1 hPa. Small yellow circles in each plot indicate NDBC buoys 46011, 46023, 46062, and 46054.

between Cape Mendocino and Point Conception, except at the San Francisco gap [*Overland*, 1984; *Halliwell and Allen*, 1987; *Beardsley et al*., 1987; *Dorman et al*., 2013]. The above factors set the large-scale summer wind pattern of equatorward flow intensified at the coast.

The large-scale wind pattern is modified downstream of major coastal capes due to hydraulic effects. The MBL, capped by the air temperature inversion layer, supports hydraulic flow dynamics when the mean MBL wind speed exceeds the speed of the long shallow water waves supported by the MBL, i.e., the flow is supercritical: the Froude number (Fr), based on the MBL layer depth and the density difference between the MBL and the overlying warm, dry air, is >1 [*Winant et al*., 1988; *Samelson*, 1992]. However, substantial hydraulic effects also occur when the Froude number is transcritical, $0.5 < \mathrm{Fr} < 1.0$ [*Rogerson*, 1999]. During the summer, the mean coastal MBL conditions between Cape Mendocino and Point Conception typically are transcritical. Hydraulic effects are generated by the equatorward MBL flow interacting with each of the five large capes in southern Oregon and California (Figure 1). The flow in the MBL slows, and the MBL thickens, on the upwind side of each cape: an MBL hydraulic compression bulge. The flow in the MBL accelerates, and the MBL thins, on the downwind side: an MBL hydraulic expansion fan [*Edwards et al*., 2001; *Pickett and Paduan*, 2003; *Koračin et al*., 2004]. For these reasons the fastest wind speeds, both in the mean and during individual events, are within $\sim$15 km of the coast and on the down-wind side of a major cape. Aircraft studies have revealed the intensified winds within 10s of km of the coast in the lees of the capes on synoptic time scales: Cape Blanco in Oregon and Cape Mendocino in California [*Dorman et al*., 2000], Pt. Arena [*Beardsley et al*., 1987; *Winant et al*., 1988; *Enriquez and Friehe*, 1995], Pt. Sur [*Dorman et al*., 1999], and Pt. Conception in California [*Dorman and Winant*, 2000; *Parish et al*., 2014]. Satellite vector wind data indicate the summer mean wind is intensified equatorward of Capes Blanco and Mendocino and Point Arena and underestimated by operational forecast modeling [*Perlin et al*., 2004].

There is also a large-scale expansion fan of the same spatial scale as California, due to the bend in California at 40°N. Its effect is to intensify the winds in the MBL for hundreds of km offshore (Figure 1) [*Edwards*, 2000]. Therefore, hydraulic control of the MBL by the large-scale bend in California is what sets the cross-coast scale of the intensified winds in the California Current Upwelling System [*Edwards et al*., 2002].

1.3. Wind Fluctuations in the California Current System

The prevailing summer upwelling-favorable wind conditions reviewed above (Figure 1) are modulated by periods of weak or reversed wind. Between Cape Blanco and Point Conception, approximately once or twice a month the equatorward wind state is interrupted within 100 km of the coast by weak winds (<3 m s^{-1}) that last 2–4 days and occasionally longer [*Halliwell and Allen*, 1987; *Beardsley et al*., 1987; *Lentz et al*., 1987;

Dorman and Winant, 1995; *Dorman et al*., 2000, 2006, 2013]. During these events, in some areas the wind may become downwelling-favorable. These summer wind events affect areas of the coast up to 1000–1500 km in length, but more typically 400–600 km [*Halliwell and Allen*, 1987]. Wind fluctuations also occur poleward of Cape Blanco, but in summer the winds poleward and equatorward of the California/Oregon border are poorly correlated [*Halliwell and Allen*, 1987].

These fluctuations in the prevailing summer winds on scales of 100s of km are caused by propagating cyclones interacting with the NPH in a synoptic sequence that can repeat throughout the summer [*Halliwell and Allen*, 1987; *Bane et al*., 2005, 2007]. First, a cyclone passes poleward of the NPH and weakens or reverses the wind to downwelling-favorable off Washington and Oregon. The cyclone may have an attached, trailing front that subsequently reverses the wind to downwelling-favorable off northern California as far south as Pt. Arena. Some of the cyclones are weaker midlevel low pressure systems and do not lead to strong downwelling-favorable winds off Oregon/N. California, but still cause wind relaxation off Oregon/N. California. Second, after the cyclone passes poleward of the NPH, and after passage of any trailing cold front, the NPH extends to the northeast. This causes intensification of the upwelling-favorable wind along the California coast. The NPH extension strengthens the pressure gradient between the NPH and the heat low over the desert southwest (section 1.2) and therefore the equatorward, upwelling-favorable coastal winds [*Halliwell and Allen*, 1987; *Bond et al*., 1996; *Nuss et al*., 2000; *Nuss*, 2007; *Taylor et al*., 2008]. The along-coast atmospheric pressure gradient strengthens by about the same factor as the change in wind velocity: if the pressure gradient doubles, the wind velocity doubles [*Halliwell and Allen*, 1987]. These cyclones followed by NPH extensions have been termed "event cycles" [*Halliwell and Allen*, 1987].

Occasionally, the northeastward extension of the NPH can then cause wind reversal along California [*Bond et al*., 1996; *Mass and Bond*, 1996; *Nuss et al*., 2000; *Nuss*, 2007]. Warm desert air can be advected offshore by the anticyclonic circulation associated with the NPH extension, causing a low-pressure area offshore of central California [*Mass and Bond*, 1996; *Nuss*, 2007]. This low pressure causes a poleward along-coast pressure gradient anomaly offshore of south/central California that can be strong enough to reverse the prevailing winds. When the offshore flow of warm air is strong enough, it leads to a coastally-trapped, propagating wind reversal [*Mass and Bond*, 1996; *Nuss*, 2007]. When the offshore flow of warm air and the other features in the synoptic pattern are weaker, the wind may reverse but not form a propagating coastally-trapped feature [*Nuss*, 2007]. Most of these events take place off northern California north of Pt. Arena. Downwelling-favorable wind events are more common near the California-Oregon border than south of Pt. Arena to Pt. Conception [*Halliwell and Allen*, 1987; *Bond et al*., 1996].

Within 10s of km of the coast, wind reversals initiated by the synoptic-scale pressure anomalies may be modified or intensified by smaller-scale dynamics, such as MBL hydraulics about each major cape [*Dorman et al*., 2013], Kelvin wave propagation in the air temperature inversion [*Ralph et al*., 1998], or gravity currents or atmospheric trapping (reviewed in *Nuss et al*. [2000] and *Nuss* [2007]). The result can be a strong, "coastally trapped" wind reversal that propagates along the coast [e.g., *Mass and Bond*, 1996; *Bond et al*., 1996]. These strong, propagating reversals occur during a subset of the synoptic-scale wind relaxation events that affect the California Current upwelling system, and mesoscale atmospheric dynamics are important in the poleward propagation of a trapped wind reversal. However, synoptic-scale pressure gradients remain important, as follows.

The poleward extent of a wind reversal can be limited by an opposing synoptic-scale pressure gradient force. An example is the wind relaxation of 22–25 June 2006 near Cape Mendocino, which was studied with aircraft flights, satellite observations, and numerical modeling [*Parish et al*., 2008; *Rahn and Parish*, 2008; *Rahn and Parish*, 2010]. This atmospheric event became coastally-trapped (a "southerly surge") and propagated poleward to Cape Mendocino as a density current, not a Kelvin wave [*Parish et al*., 2008; *Rahn and Parish*, 2008]. Satellite images show the associated stratus cloud tongue propagated north from Monterey Bay to Cape Mendocino on 22–23 June but remained at Cape Mendocino over 24–25 June when the poleward extension of this event was halted by an opposing synoptic-scale atmospheric pressure gradient [*Rahn and Parish*, 2010]. Data from several aircraft flights within ~60 km offshore of the coast near Cape Mendocino revealed the atmospheric boundary layer structure of the narrow northern nose of the arrested density current and associated area of weak winds. When combined with a numerical model of the event, the aircraft data indicated the density current stopped propagating northward at Cape Mendocino not due to topographic blocking by the coastline protrusion of the Cape but due to an equatorward pressure gradient force (PGF) that existed in the ambient atmospheric boundary layer to the north of Cape Mendocino

[*Rahn and Parish*, 2010]. Therefore, synoptic-scale pressure anomalies are important factors in ending even the wind reversals that become coastally-trapped.

1.4. Wind Relaxations at Pt. Conception

Although wind reversal to downwelling-favorable is rare at Pt. Conception in summer (section 1.3), wind relaxation is common. Wind relaxations at Pt. Conception have been studied in the context of the oceanic "relaxation flow" state that occurs in the Santa Barbara Channel [*Harms and Winant*, 1998; *Winant et al*., 2003; *Dever et al*., 1998; *Dever*, 2004] and the poleward warm ocean currents that originate in the Channel and flow past Pt. Conception [*Melton et al*., 2009; *Washburn et al*., 2011]. Wind relaxations at Pt. Conception occur in all months of the year, but are most common in late summer [*Melton et al*., 2009].

In contrast to the wind relaxations/reversals farther poleward in the California Current system, which are often followed by intensification of the prevailing upwelling-favorable winds (section 1.3), the Pt. Conception wind relaxations tend to be immediately preceded by wind intensification [*Melton et al*., 2009; *Washburn et al*., 2011]. For example, before the wind relaxation of 14 June 2001, at the 3 National Data Buoy Center (NDBC) buoys just northwest of Pt. Conception (Figure 1) the wind velocities were $\sim$10 m s^{-1} equatorward for $>$3.5 days, twice as strong as the mean wind velocity [*Melton et al*., 2009]. At buoy 46054 in the western Santa Barbara Channel, in the region of intense winds south of Pt. Conception (section 1.2), the wind velocity was 15 m s^{-1} for several days before the wind relaxation. At all 4 buoys, during the relaxation the wind velocity weakened to near 0 m s^{-1} for several days. Below, we will show that wind relaxations at Pt. Conception are due to weaker versions of the same synoptic sequence that causes the rarer wind reversals described by *Halliwell and Allen* [1987].

Poleward winds along the coast in the Southern California Bight, including in the Santa Barbara Channel east of Pt. Conception, can occur during Catalina Eddy events. Those events, which last $\sim$2 days, involve a cyclonic eddy in the atmosphere occupying the Southern California Bight [e.g., *Bosart*, 1983]. However, the wind relaxations at Pt. Conception do not correspond directly to Catalina Eddy events. During Catalina Eddy events, the prevailing winds at Pt. Conception can remain strongly upwelling-favorable [e.g., *Mass and Albright*, 1989; *Hu and Liu*, 2002], rather than relaxing as during the events studied here. Occasionally, Catalina Eddy events may lead to coastally-trapped atmospheric disturbances that propagate poleward out of the Southern California Bight, resulting in weak winds at and poleward of Pt. Conception due to the coastal trapping; model results suggest this can happen if the prevailing winds impinging on the Bight become northeasterly [*Skamarock et al*., 2002]. In general, however, in summer the winds poleward and equatorward of Pt. Conception are poorly correlated [*Halliwell and Allen*, 1987]. The focus of our study is on the general class of wind relaxation events at Pt. Conception in which the wind velocity falls below the mean, not on the subset of relaxations that may be related to Catalina Eddy events.

1.5. The Oceanic Response to Wind Relaxation

In summer, weakening or reversal of the prevailing upwelling-favorable wind can drive reversal of the oceanic flow near the coast. Off Oregon and northern and central California, wind relaxations and reversals are observed to lead to poleward oceanic flows [e.g., *Hickey*, 1979; *Chelton et al*., 1988; *Woodson et al*., 2009]. In many locations, weakening of a prevailing upwelling-favorable wind is sufficient to enable reversal of the oceanic flow; wind reversal is not required. This is because poleward oceanic pressure gradients, driven by sea-level and water density differences, are generated in the lee of coastline protrusions during upwelling-favorable wind forcing [*Gan and Allen*, 2002a,2002b]. When the wind weakens, the oceanic pressure gradient force accelerates the water poleward even if the wind does not reverse to poleward. Warm poleward oceanic flows are observed along northern California north of Pt. Reyes when the upwelling-favorable wind weakens but does not reverse [*Lentz et al*., 1987; *Send et al*., 1987]; *Largier et al*., 1993]. Similar poleward buoyant flows are observed poleward of coastline bends in other eastern boundary upwelling systems, including off Iberia [*García-Lafuente et al*., 2006; *Relvas and Barton*, 2002, 2005; *Garel et al*., 2016] and in the Benguela upwelling system [*Fawcett et al*., 2008].

Near Pt. Conception, poleward ocean flows during weakened upwelling-favorable winds are common [*Dever et al*., 1998; *Harms and Winant*, 1998; *Winant et al*., 2003; *Dever*, 2004; *Cudaback et al*., 2005; *Melton et al*., 2009; *Nidzieko and Largier*, 2013]. Although the wind typically does not reverse direction, when the wind velocity falls below its mean value buoyant warm water from the Santa Barbara Channel moves

poleward around Pt. Conception [*Melton et al*., 2009]. The oceanic flow is due to an oceanic poleward pressure gradient force (with both barotropic and baroclinic components) that overcomes the equatorward wind stress forcing at Pt. Conception when that wind stress weakens [*Washburn et al*., 2011]. The oceanic pressure gradient develops during the prevailing upwelling-favorable wind conditions, when sea level and water temperature become elevated along the mainland in the eastern Santa Barbara Channel relative to conditions north of Pt. Conception [e.g., *Harms*, 1998]

The poleward oceanic flows at Pt. Conception cause warm water to propagate northward against the prevailing currents, with important ecological implications including larval transport and large coastal water temperature anomalies. The poleward flows may be an important mechanism for larval transport along the central coast of California [*Wilson et al*., 2008] and from the Southern California Bight poleward past Pt. Conception, which is a biogeographic range boundary for some intertidal species but not others [*Blanchette et al*., 2008]. Poleward warm flows have also been implicated in larval delivery to the coast off Oregon [*Dudas et al*., 2008] and northern California [*Wing et al*., 1995a,b; *Mace and Morgan*, 2006a,b]. The buoyant poleward flows at Pt. Conception cause substantial water temperature anomalies. Over a distance of ∼10–50 km north of Pt. Conception and occasionally farther, within ∼15 km of the coast the cold, previously upwelled water is replaced over a period of hours by water several degrees warmer from south and east of Pt. Conception that remains at the coast for several days [*Washburn et al*., 2011]. Understanding the wind relaxations that lead to the warm poleward flows at Pt. Conception is important for understanding the physical dynamics that affect ecosystems in the California Current system and other eastern boundary upwelling systems.

1.6. The Purpose of This Study

The wind patterns during wind relaxations and reversals off Oregon and California have been studied using buoy winds, land-based measurements and soundings, automated coastal stations, and aircraft. Due to the difficulty of obtaining wind stress measurements over a spatial area as large as the entire west coast of North America from aircraft or buoys, most previous studies of wind relaxations have focused within 100 km of a single major cape [*Winant et al*., 1988; *Rogers et al*., 1998; *Rahn and Parish*, 2010], with rare exceptions to ∼190 km offshore [*Rogers et al*., 1998]. Previous satellite-based studies of the wind field off the West Coast included wind speed but not direction [e.g., *Edwards et al*., 2002], covered a subset of the major capes [*Perlin et al*., 2004], or focused on intense upwelling-favorable winds, not relaxations or reversals [*Taylor et al*., 2008]. Previous studies of the synoptic forcing of wind fluctuations, reviewed in section 1.3, have focused on strong wind reversals and on distinguishing the dynamics of Kelvin wave-like events, gravity current disturbances, and synoptic scale wind reversal events that can be coastally trapped (e.g., reviewed in *Nuss et al*. [2000]). In contrast, our focus is on determining the synoptic-scale forcing associated with the weaker, but oceanographically important, wind relaxations at Pt. Conception, events during which the wind typically does not reverse at Pt. Conception.

In the past 15–20 years, satellite-based vector wind velocity data have become available that permit us to study the vector wind stress field almost simultaneously over the entire California Current upwelling region. Though the spatial detail in satellite data is not as fine as that available in aircraft studies, satellite vector wind data provide a complementary view to aircraft- or buoy-based studies, recording the wind stress over the entire California Current upwelling system with a spatial resolution of ∼40 km. We focus on the years 2000–2009, when QuikSCAT satellite data are available during summer.

The purpose of this study was to determine (1) the spatial extent of the wind relaxations that affect Pt. Conception, (2) the synoptic forcing that causes the relaxations, and (3) whether the Pt. Conception wind relaxations are related to wind events farther poleward in the upwelling system. We focused on May–August, when oceanic poleward flows at Pt. Conception are also common [*Washburn et al*., 2011]. Section 2 describes the data and how we identified the times of wind relaxations and constructed composite averages of the atmospheric data during relaxation events. Section 3 presents the progression of the wind events along the coast, an example of a single wind relaxation, the composite space and time evolution of 67 wind relaxations during May–August 2000–2009, and the regional atmospheric conditions associated with wind relaxations that affect the Pt. Conception area. Section 4 discusses the cause of the Pt. Conception relaxations and what sets the spatial scale of the relaxed winds. Section 5 contains our conclusions.

2. Data and Methods

2.1. Atmospheric Data

2.1.1. Buoy Winds

We used three types of wind data. The first type of data is from NDBC meteorological monitoring buoys, accessible at http://www.ndbc.noaa.gov. The four main buoys are located near Pt. Conception, California in the region of summertime prevailing upwelling-favorable winds (Figure 1). One buoy, 46054, is in the western Santa Barbara Channel. The other three buoys, 46011, 46023, and 46062, are located 10–20 km north of Pt. Conception and 10–20 km offshore. The winds at the four buoys are highly correlated on time scales of days to weeks [*Dorman and Winant*, 2000; *Melton et al*., 2009]. We used the hourly wind velocity data from 2000 to 2009 and calculated equivalent 10 m wind velocity and wind stress using the time-varying anemometer heights and the neutral stability COARE 3.5 algorithm [*Edson et al*., 2013].

2.1.2. Satellite Vector Winds

Our second source of wind data was the microwave scatterometer SeaWinds on the QuikSCAT satellite. This instrument returned vector wind stress over the ocean from 1999 to 2009 based on active microwave sensing of backscatter from ocean surface roughness and an empirical relation between that backscatter and the surface wind stress or 10 m equivalent neutral winds [*Ricciardulli and Wentz*, 2011]. One advantage of QuikSCAT for oceanographic studies is that its backscatter measurement is directly related to the wind stress at the ocean surface. That wind stress is more relevant for ocean dynamics than the wind velocity measured several meters above the surface from an NDBC buoy, though both are usually converted to 10 m equivalent winds. Wind stress data are not available from QuikSCAT during heavy rain events due to the confounding effects of rain and wind on surface roughness. However, rain events are rare in summer in our focus region off central and southern California.

Our study region is 25°N to 50°N and 110°W to 140°W (Figure 1), though a smaller region that captures the major patterns is shown in some figures below. We used the 10 m equivalent neutral wind velocity QuikSCAT Version 3 Level 2B data ("L2B data") produced by NASA's Jet Propulsion Laboratory [*Fore et al*., 2014], which covers October 1999 to November 2009, available at http://podaac.jpl.nasa.gov/dataset/QSCAT_LEVEL_2B_OWV_COMP_12. The QuikSCAT data are in 1800 km-wide "swaths." Each swath represents one pass of the QuikSCAT satellite and each is provided on a different 12.5 km grid. We calculated wind stress from the 10 m equivalent neutral wind velocity using the COARE 3.5 neutral drag parameterization [*Edson et al*., 2013]. We then linearly interpolated the data onto a 0.1° latitude-longitude grid using Delaunay triangulation, using only swath points where the quality flags indicated all 4 "flavors," or combinations of 2 signal polarizations and 2 satellite viewing angles, of backscatter observation were available (see *Fore et al*. [2014] and the QuikSCAT User Guide, ftp://podaac-ftp.jpl.nasa.gov/allData/quikscat/L2B/docs/QSUG_v3.pdf, for details). The effective spatial resolution of the L2B data is ∼40 km, so the gridded data are oversampled. We kept the individual QuikSCAT swaths, one per pass of the satellite over a given location, separate. The temporal resolution is ∼12 h. There are 17 gaps in the data that last 0.5–3 days.

Morning and evening satellite passes were treated separately and then averaged in the analysis below. QuikSCAT has a sun-synchronous polar orbit, yielding data approximately twice per day, with equator crossings near 6 am and 6 pm local time: the ascending and descending passes, respectively. When forming averages over many passes, we averaged morning passes together and separately average evening passes together, then averaged the morning and evening results together. This is necessary because near the coast, some grid points have more data from morning than evening passes or vice versa. Our method weights morning and evening passes equally, preventing the result near the coast from being biased toward one part of the diurnal cycle. The wind stress near the coast is significantly weaker in the morning than the evening [*Beardsley et al*., 1987; *Dorman and Winant*, 1995]. Our method also averages out much of the effect of the diurnal cycle, which is not the focus of this study.

2.1.3. Reanalysis Products

The third source of wind data is a reanalysis product, a dynamically consistent blend of model and observations. We used the National Center for Environmental Prediction (NCEP) North American Regional Reanalysis A (NARR) [*Mesinger et al*., 2006] output for 2000–2009, available from http://www.ncdc.noaa.gov. The temporal resolution is 3 h, the spatial resolution is ∼32 km, and the spatial coverage is of North America and the adjacent ocean, including our entire study region. We use the wind stress at sea level, the atmospheric pressure at sea level (atmospheric pressure reduced to mean sea level, "SLP"), and the height of the

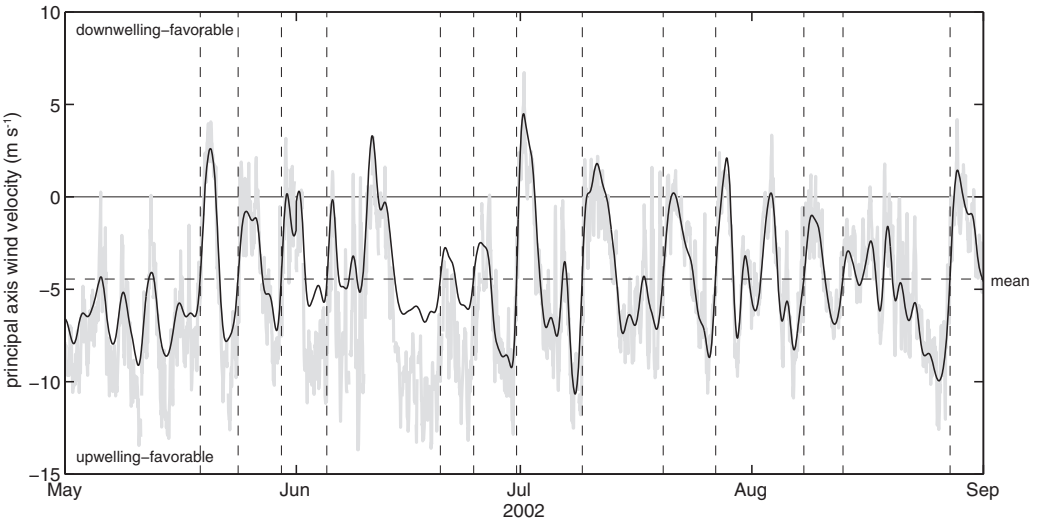

Figure 3. An example of wind relaxation events at Pt. Conception during summer 2002. Grey: hourly principal axis (∼along-coast) wind velocity at NDBC buoy 46011 near Pt. Conception. Black: first EOF of low-pass filtered along-coast wind velocity at buoys 46011, 46023, 46062, and 46054, with the mean wind velocity added (the mean of the EOF is zero). Vertical dashed lines mark times of wind relaxations as identified by the *Melton et al.* [2009] index: times when the EOF crosses zero, i.e., the wind velocity drops below its mean value, after being strongly upwelling-favorable for ∼2 days.

500 hPa, or -mb, pressure surface (500 hPa geopotential height analysis). We also examined the 700 hPa height fields (not shown); the features were similar to those discussed here for the 500 hPa height. QuikSCAT wind directions are nudged toward NCEP global model wind directions [*Fore et al.*, 2013], but the amplitude of QuikSCAT wind is independent of NCEP. The NARR reanalysis does not assimilate QuikSCAT data, so the two products are nearly independent.

2.2. Identifying the Times of Wind Relaxations

We identified the time of onset of wind relaxations using the *Melton et al.* [2009] method. This method is based on finding the zero crossings of the first empirical orthogonal function (EOF) of the 36 h low-pass filtered along-principal-axis, or roughly along-coast, wind velocity at the 4 NDBC buoys near Pt. Conception (Figure 1). When the EOF crosses zero, that indicates the wind velocity is falling below its mean value. For an event to qualify as a relaxation, the wind velocity is required to stay below the mean $\geq$60% of the time for the next 2.5 days.

As an example, all wind relaxation start times identified by the Melton index for the year 2002 are shown in Figure 3 (dashed vertical lines). Though the Melton index identifies events throughout the year, we studied events in May–August. We extended the *Melton et al.* [2009] index to 2000–2009, the time period of the QuikSCAT mission, and identified 82 wind relaxations at Pt. Conception during May–August. Below, we examine the anomalies of wind stress from QuikSCAT and buoys and SLP and 500 hPa height from NARR during 67 of those events, as compared to the mean wind stress, SLP, and 500 hPa height during all days in May–August 2000–2009.

Similarly to previous studies [e.g., *Mass and Bond*, 1996; *Nuss*, 2007], we rejected ∼15–20% of the wind relaxation events identified by the buoy index. These rejected events, 15 out of a total of 82 relaxations identified initially, are associated with landfalling fronts. (*Mass and Bond* [1996] also rejected synoptic wind reversals associated with troughs or cyclones, which we do not.) The landfalling fronts typically cause the wind to relax or reverse almost simultaneously (within ∼1 day) along 100s or 1000s of km of coastline. The dynamics and effects of strong landfalling fronts are not the subject of this study.

2.3. Constructing Means and Anomalies of Wind and Pressure

To determine the evolution of the wind relaxations and their spatial and temporal extent, we constructed conditionally averaged anomalies of wind stress, atmospheric pressure, and geopotential height (height of the 500 hPa pressure surface). We constructed the anomalies in four steps. In step 1, we identified the times

of wind relaxations near Pt. Conception using the *Melton et al*. [2009] method (section 2.2). The times of wind relaxations identified from the EOF form the buoy event index.

In step 2, we calculated the composite mean wind and pressure fields over the 67 wind relaxations. To do this, we phase-averaged the QuikSCAT wind stress or NARR SLP or 500 hPa height data based on the buoy event index. We selected data from 10 days before to 10 days after each wind relaxation and averaged the data from all 67 wind relaxations together for each 12 h of the wind event. This yielded the mean QuikSCAT wind stress field every ~12 h and NARR fields every 12 h, aligned in time relative to the start of a wind relaxation. We then averaged together the morning and evening composite wind stress fields from each day. The result is a composite image for the time when a wind relaxation is beginning at Pt. Conception (day 0), one day before a wind relaxation begins (day −1), two days before (day −2), etc. In each map, QuikSCAT data are only displayed for grid points where data were available for at least 10 of the 67 wind relaxations. To make the NARR fields comparable to the QuikSCAT fields, we used the NARR data closest in time to each QuikSCAT pass at Pt. Conception rather than using all NARR data from a given day. In this way, we calculated the temporal progression of the wind field from 10 days prior to 10 days after the start of a wind relaxation at Pt. Conception.

In step 3, we calculated the mean wind stress, SLP, and 500 hPa height over all days in May–August 2000–2009 (Figure 2), again only displaying data at locations with $>=10$ measurements available. Similarly to the composites in step 2, we calculated the means separately for the ascending and descending QuikSCAT passes, producing morning and evening means, and then averaged the results together to form a single mean for each day.

In step 4, we calculated the composite wind and pressure anomalies for 10 days prior to 10 days after a wind relaxation by subtracting the mean (step 3) from the conditional average fields (step 2). We then determined when and where the anomalies are different at the 95% confidence level from the May–August mean. Below, only data from 6 days before to 5 days after the wind relaxation onset time are shown. The anomalies on days farther from the event time were small and generally not significantly different from the mean. We defined weak wind stress as < 0.03 Pa, which in the case of neutral atmospheric stability corresponds to a wind speed < 5 m s^{-1}, well below the high wind threshold of 8 m s^{-1} used by, e.g., *Edwards et al*. [2002].

In section 3.4 below, we show the composite wind stress anomalies relative to the summer mean wind stress. The wind stress anomaly is a vector, but we display only the component in the direction of the mean May–August wind stress at each grid location, i.e., the directions of the arrows in Figure 2a. The wind stress anomalies in the cross-mean direction during these wind events are weak ($<$ 0.03 Pa; not shown). Negative wind stress anomaly indicates the upwelling-favorable wind stress is weaker than the May–August average; the actual wind stress may be weakly upwelling-favorable or reversed to downwelling-favorable. Grey shading indicates the anomaly is not significant at the 95% confidence level as compared to the mean wind stress at that location in Figure 2.

3. Results

3.1. Wind Stress Patterns Along the Coast

We first consider the patterns of wind stress along the coast, conditionally averaged relative to the onset of the Pt. Conception relaxation. The wind events that result in relaxations at the buoys near Pt. Conception are not confined to the Pt. Conception area. The wind weakens over 100s of km of coastline (blue in Figure 4). In addition, the satellite and buoy data show a robust three-stage pattern of wind features that are coherent in space and associated in time.

Stage 1 is a weakening or reversal of the wind in the poleward part of the upwelling system. During days −6 to −2 relative to the onset of the Pt. Conception wind relaxation, the composite wind stress off Oregon and northern California is significantly less than the mean (blue in Figure 4, day −6 to −2). Stage 1 may involve wind reversal, but is not necessarily a coastally-trapped wind event or "southerly surge," and does not necessarily involve poleward propagation of the wind anomaly. On average, the wind at the buoys does not reverse direction (Figure 4).

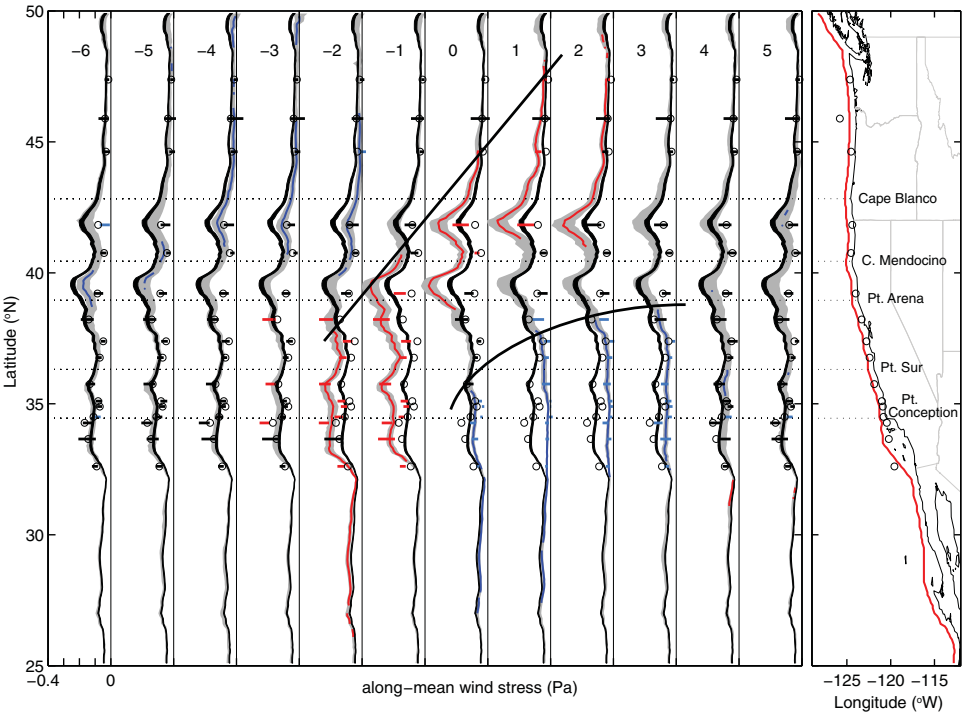

Figure 4. (See previous page for figure.) Temporal evolution of the composite wind relaxation event along the coast, based on 67 wind relaxations in May–August 2000–2009. Wind stress is shown from QuikSCAT (along the red line in the far right plot) and NDBC buoys (black circles in far right plot). The left plot shows wind stress as a function of latitude, composited daily for 6 days before to 5 days after the relaxation (day 0), as indicated in the upper part of each plot. The vertical axis is offset horizontally for each day; thin vertical lines are reference zero lines for each wind stress plot. The scale, at bottom left, is the same for all wind stress plots. Horizontal dotted lines mark the latitudes of the 5 major capes. Red (blue) indicates the wind stress is significantly greater (less) than the May–August mean. *QuikSCAT*: The filled black area is the same for each day and indicates a 95% confidence interval around the mean May–August 2000–2009 wind stress from QuikSCAT. The filled grey areas indicate 95% confidence intervals around the wind stress during each day of the composite. Red and blue lines indicate the composite QuikSCAT wind stress when it is significantly different from the summer mean (black). *Buoys*: Black circles indicate mean wind stress during May–August 2000–2009. Black, red, and blue bars indicate 95% confidence intervals for wind stress at buoys during relaxations (not different from, significantly greater than, and significantly less than the mean, respectively). Curved black lines indicate the approximate poleward limit of the wind intensification (red) and the southern/central California wind relaxation that affects Pt. Conception (blue in day 0–5).

Stage 2 is an intensification of upwelling-favorable winds over the entire California Current upwelling system. During days −3 to +2, the upwelling-favorable winds near the coast are stronger than the mean beginning in the equatorward part of the upwelling system, i.e., central California, and shifting poleward with time (red in Figure 4).

Stage 3 is a weakening of the wind stress from Pt. Conception to Pt. Arena (Figure 4, blue in day 0–4). This wind relaxation affects the Pt. Conception area and is the wind relaxation we set out to study. However, it is stage 3 of a wind pattern that affects the entire California Current upwelling system. Wind stresses at the NDBC buoys along the coast agree with the three-stage pattern in the satellite data (circles and red/blue bars in Figure 4).

3.2. Spatial Extent of the Wind Stress Anomalies

In this section, we discuss the temporal and spatial patterns of the wind stress offshore of the coast by analyzing the wind stress anomalies (section 2.3) relative to the summer mean.

3.2.1. The Wind Relaxation of 14 June 2001

We first present QuikSCAT wind stress fields from the wind relaxation of 14 June 2001, which caused a poleward oceanic flow at Pt. Conception [*Melton et al.*, 2009]. The wind stresses during days −4, 0, and 1 of the relaxation are shown in Figures 5a, 5c, and 5e. The corresponding anomalies relative to the mean in Figure 1 are shown in Figures 5b, 5d, and 5f to orient the reader to the anomalies shown in later figures. The 3 stages of the composite wind pattern (section 3.1 and Figure 4) are visible in this individual event. Stage 1,

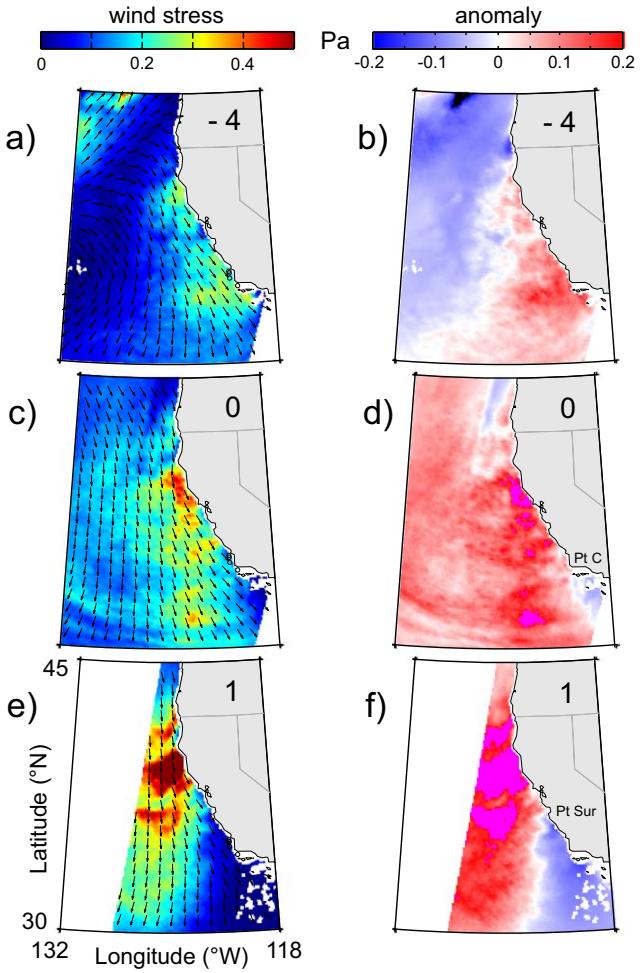

Figure 5. (a, c, e) Wind stress from QuikSCAT ascending (~6 am local time) passes during days −4, 0, and 1 of the relaxation event that began at Pt. Conception on 14 June 2001, plotted similarly to Figure 1. (b, d, f) The corresponding wind stress anomalies, relative to the mean wind stress in Figures 1 and 2a, calculated as described in section 2.3. Only the component of the wind stress anomaly parallel to the local mean wind direction at each grid point (Figure 1a) is shown. Anomalies greater than the color scale range of 0.3 Pa are shown in magenta. The anomaly is shown 4 days before and 0 day and 1 day after the wind relaxation time at Pt. Conception, as indicated in the upper right of each plot. White strips with straight edges are regions of no data outside the QuikSCAT swaths. Where multiple overlapping QuikSCAT swaths are available during a single 12 h period (rarely), the more recent data are plotted over the older data.

weakened or reversed winds off Oregon, is the blue area along the coast in Figure 5b. Stage 2, intensified upwelling-favorable winds, is the red areas in Figures 5b, 5d, and 5f. Stage 3, the wind relaxation at Pt. Conception, is the blue area in Figures 5d and 5f. During the morning satellite pass on day 0 (Figure 5c) the relaxed winds were confined to the Southern California Bight (SCB) southeast of Pt. Conception. This is more apparent in the map of wind stress anomaly relative to the May–August mean (blue area in lower right of Figure 5d). By the following day, the area of weakened winds extended to Pt. Sur and ~200 km offshore of Pt. Conception (Figures 5e and 5f).

3.2.2. Anatomy of the Composite Wind Relaxation

Here we describe the average time progression and spatial extent of the three stages using the composite mean wind stress anomalies from the 67 wind relaxations at Pt. Conception in May–August 2000–2009 (Figure 6). The number of wind relaxations averaged to form each plot in Figure 6 can be less than 67, depending on QuikSCAT data availability. North of ~45°N, multiple overlapping QuikSCAT swaths are occasionally available in one 12 h period. In those cases data from the two swaths are averaged together, not overwritten as in Figure 5, to take advantage of all wind data available during the event. We examined the wind stress anomalies for 10 days before to 10 days after the onset of the wind relaxation at the Pt. Conception buoys (day 0). During days −10 to −7 and days +7 to +10, the composite wind stress anomaly is not significantly different from zero anywhere in the study area. Only days −6 to +5 are shown below because these days span the three stages.

3.2.2.1. Stage 1: Weakening or Reversal of the Wind Off Oregon and Northern California

The weakening or reversal off Oregon, centered at Cape Blanco, lasts 5 days in the composite (Figure 6, days −6 to −2) and extends >200 km offshore. Individual events can last less than 5 days (2–3 days is the typical timing reported by *Bane et al.* [2005, 2007]) and may be stronger than in the composite, but have start times that vary relative to the start of the Pt. Conception wind relaxation that defines day 0 in this analysis. For example, Stage 1 ended by day −3 in a 21 June 2006 event but lasted through day 0 in the 13 June 2000 event (not shown). The relative timing of events off Oregon that precede the 67 individual California wind relaxations during May–August 2000–2009 is beyond the scope of this study. These observations, however, indicate that weakening of the wind off Oregon/northern California and wind relaxations off central/southern California tend to come in pairs, linked in time but separated by the episode of intense upwelling-favorable winds, Stage 2.

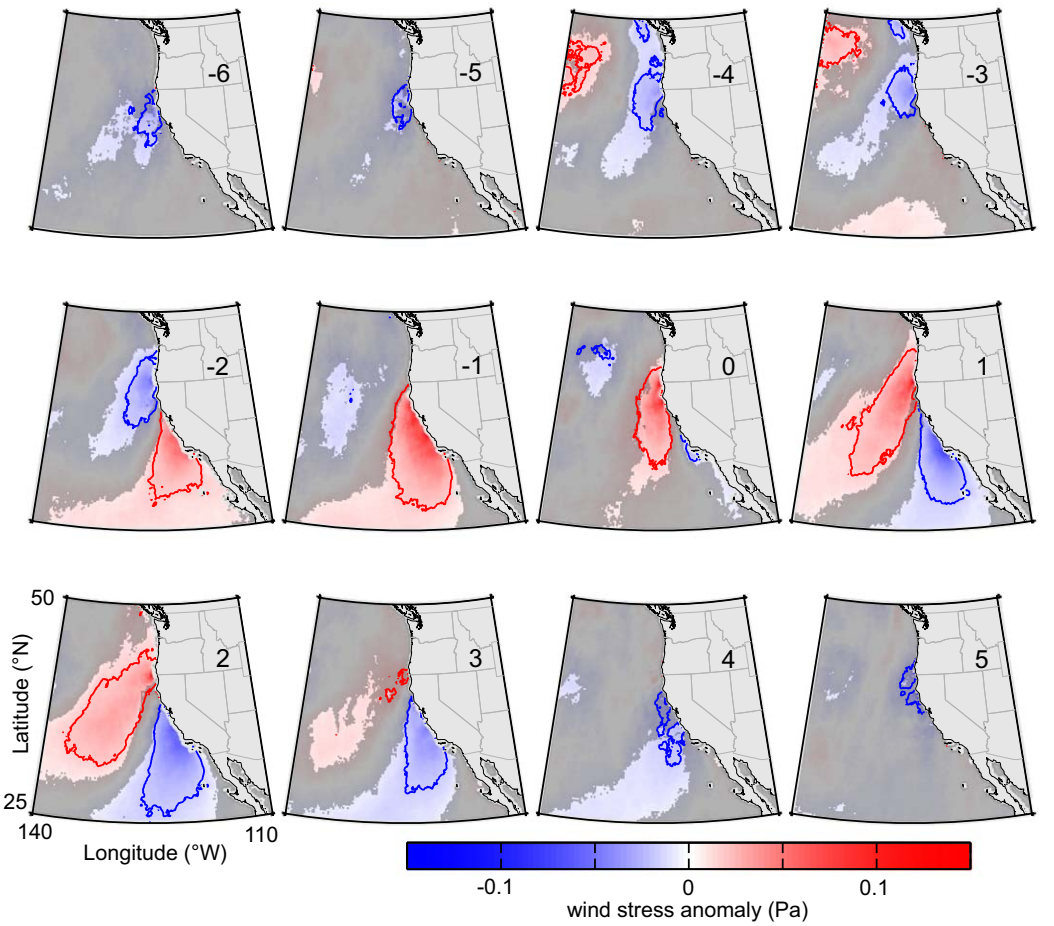

Figure 6. Evolution of wind stress anomalies for the composite wind relaxation event, based on 67 events during May–August 2000–2009. The number in each plot indicates time in days relative to the onset of wind relaxation at the Pt. Conception buoys (day 0). Color indicates the wind stress anomaly in the direction of the mean wind stress at each point (Figure 1). Blue indicates weaker than the mean upwelling-favorable wind stress, and/or downwelling-favorable wind stress. Red indicates the upwelling-favorable wind stress is stronger than the mean in Figure 1. Red and blue contours indicate a wind stress anomaly of +/- 0.03 Pa. The cross-mean component of the wind stress anomalies is weak (not shown). Grey indicates the anomaly is not significant at the 95% confidence level. Ascending and descending swaths were averaged separately over the 67 events and the resulting 2 maps averaged together for each day (section 2.3). First a wind relaxation occurs off Oregon (blue, top row), followed by wind intensification off California and Oregon (red), followed by the wind relaxation that affects Pt. Conception (blue, bottom row).

3.2.2.2. Stage 2: Wind Intensification

The wind intensification that precedes Pt. Conception wind relaxations was noted previously at the Pt. Conception buoys [e.g., *Melton et al*., 2009], but here we detect the intensification over 100s of km of ocean offshore off central and southern California (red in Figure 6, day −2 to 2), similar to events in *Taylor et al*. [2008]. On average, 2 days before the Pt. Conception relaxation there are enhanced upwelling-favorable winds from Pt. Arena to offshore of the SCB. The area of intensified wind grows in size and moves poleward over ∼4 days, eventually resulting in enhanced upwelling-favorable wind stress off Oregon during the stage 3 wind relaxation off California (red in Figure 6, day 0–2). The enhanced upwelling-favorable winds off Cape Blanco disappear by 3 days after the start of Stage 3, the wind relaxation that affects the Pt. Conception area (Figure 6, day 3).

3.2.2.3. Stage 3: Wind Relaxation at Pt. Conception

On average, when the wind relaxation begins at the Pt. Conception buoys the wind stress is already weaker than usual in the SCB (Figure 6, day 0). The winds first begin to weaken near San Diego [*Dorman and Koračin*, 2008], which is ∼400 km southeast of the bend in the coastline at Pt. Conception. On day 0, near the coast south of Pt. Arena the winds have weakened to the annual mean summer wind stress, resulting in zero wind stress anomaly (Figure 6, day 0). There is a small area of anomalously weak wind near Pt. Conception. Then the area of weak winds extends northward and offshore with time. The wind relaxations grow in

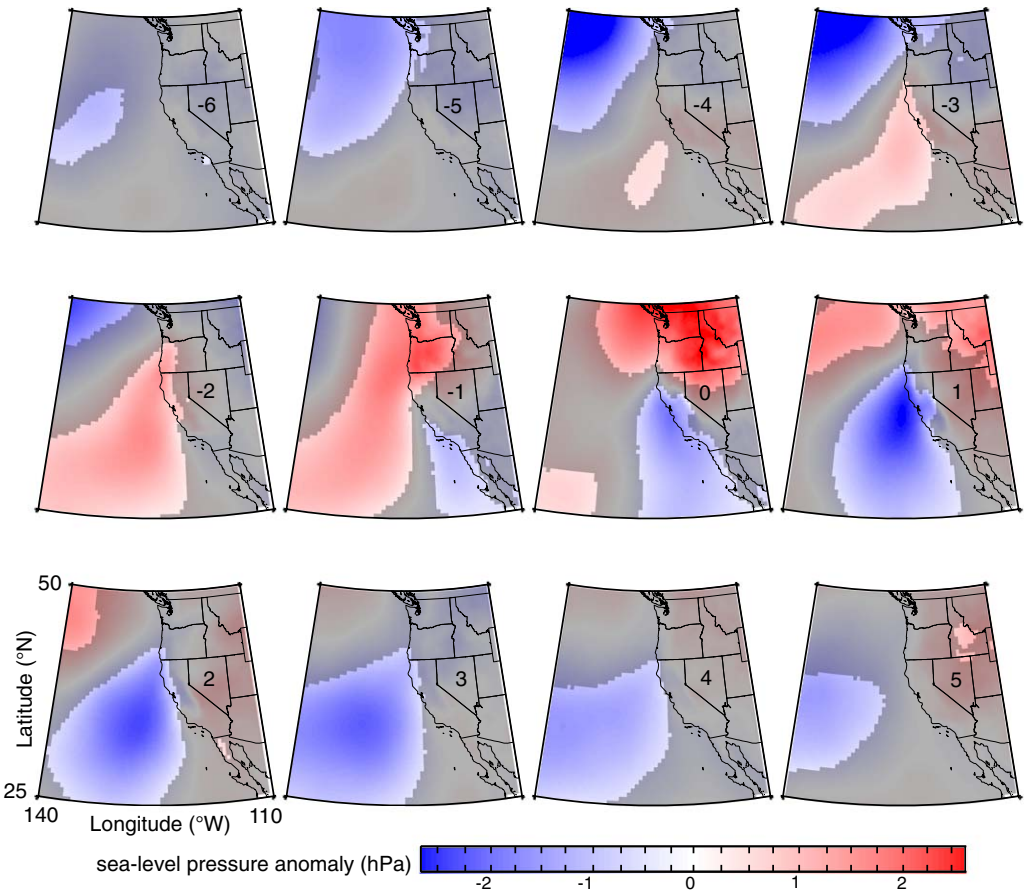

Figure 7. Composite anomalies constructed similarly to Figure 6, but for sea-level pressure from NARR.

spatial extent for ~2 days and then fade. On average, by 6 days after the Pt. Conception wind relaxation begins, the wind stress anomalies are weak (<0.03 Pa) or not significant.

At its maximum extent, the composite mean wind relaxation at Pt. Conception extends 500–1000 km offshore (blue in Figure 6, day 2). In the along-coast direction, the relaxed winds extend on average from south of the U.S./Mexico border poleward to the Pt. Arena/Cape Mendocino area (Figure 6, day 2). The wind relaxation affects an area of the ocean $O(500{,}000\ km^2)$, a region approximately the size of California. The magnitude of the strongest wind stress anomalies is as large as the magnitude of the mean wind stress off central California (Figure 2a), indicating the wind stress relaxes to near zero.

3.2.3. Interpreting the Composite Mean Event

The negative wind stress anomalies in Figure 6 may indicate weakened or reversed winds. Off Pt. Conception, on synoptic time scales the negative wind stress anomalies typically indicate weak winds but not downwelling-favorable wind stress (e.g., Figure 3). Off Oregon and northern California, the negative wind stress anomalies may indicate either weak or downwelling-favorable wind stress depending on the particular event. A detailed analysis of each of the 67 individual events is beyond the scope of this study. However, the buoy and satellite data indicate that, on average, during these events the wind stress does not reverse to downwelling-favorable anywhere along the coast (Figure 4).

A composite mean can be misleading if the individual events are not all similar. Here the composite mean wind relaxation is a good representation of the 67 individual events off Pt. Conception. In the area of relaxed winds in Figure 6, day 1–2 (blue), the standard deviation of the wind stress anomalies is smaller than the mean anomaly. This suggests the 67 events that affected the Pt. Conception area in May–August 2000–2009 are similar to each other and to the composite mean. In addition, visual inspection indicates the individual events each display a three-stage pattern similar to the mean (not shown), confirming that the composite mean in Figure 6 is a good representation of the individual events.

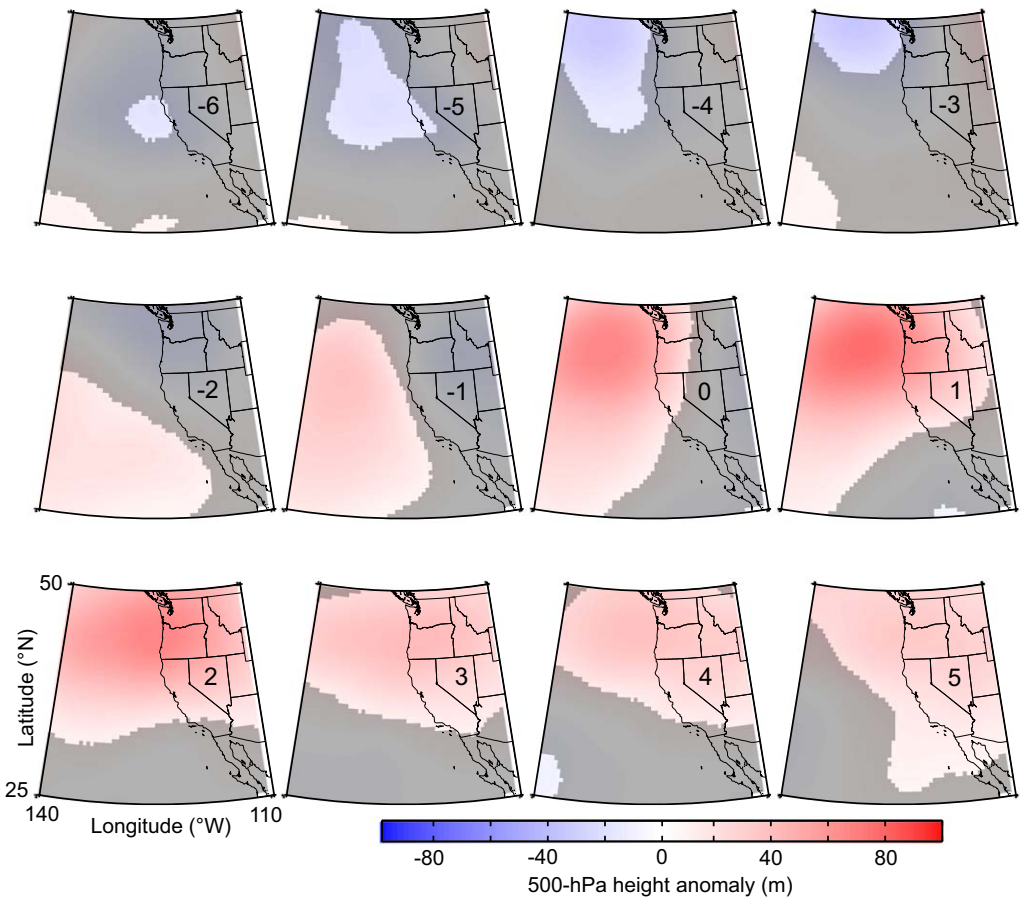

Figure 8. Composite anomalies constructed similarly to Figure 6, but for 500 hPa height from NARR.

3.3. Atmospheric Conditions Associated With Pt. Conception Wind Relaxations

To determine what synoptic atmospheric phenomena tend to be associated with Pt. Conception wind relaxations in summer, we consider the composite SLP and 500 hPa height anomalies from NARR. We focus on the SLP anomalies and the resulting PGF anomalies in the along-coast (along-mean wind stress) direction, similarly to previous studies [e.g., *Halliwell and Allen*, 1987].

During stage 1, weakened or reversed winds off Oregon, a low SLP anomaly develops off Washington and Oregon (blue in Figure 7, day −6 to −3). This surface pressure anomaly extends above the MBL into the midtroposphere and is evident at the 500 hPa level as a weak trough centered near 130°W (Figure 8, day −6 to −3). In addition, there is a high-pressure anomaly that begins off California (Figure 7, day −3) and extends to Oregon and Washington (Figure 7, day −2 to 1). Like the low SLP anomaly, the high SLP anomaly is linked to a similar midlevel feature in 500 hPa height, in this case with larger spatial extent (Figure 8, day −2 to 1). This pair of pressure anomalies can be understood as the result of a weak summer cyclone or trough followed by a poleward displacement of the NPH, equivalent to the "event cycles" that cause wind reversal off northern California (section 1.3). The paired low- and high-SLP anomalies combine to create a poleward PGF anomaly along the coast off Oregon and northern California (blue contours in Figure 9, day −6 to −1), opposing and slowing or reversing the prevailing winds off Oregon (blue shading in Figures 6 and 9, day −6 to −1).

During stage 2, the high-SLP anomaly along the coast moves poleward (Figure 7, day −2 to 1) and a second low-SLP anomaly develops off southern California (blue, day −1), later extending poleward to Cape Blanco in Oregon (day 0–3). This pair of high and low SLP anomalies creates an equatorward PGF anomaly along the coast from the high SLP to the center of the low SLP (red contours in Figure 9). This PGF strengthens the prevailing winds, consistent with the enhanced upwelling-favorable wind stress and velocity off northern California and Oregon (red shading in Figures 6 and 9).

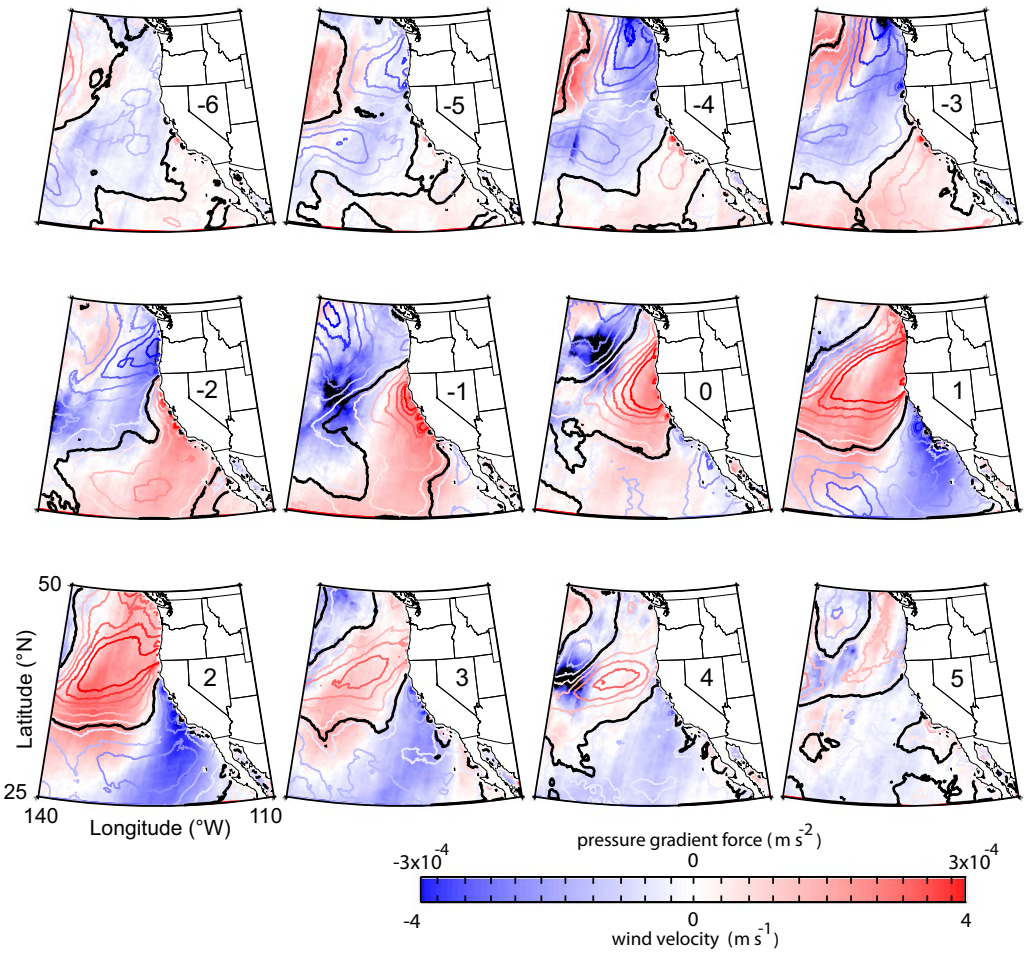

Figure 9. Composite anomalies constructed similarly to Figure 6. Shading: along-mean component of the wind velocity anomaly from QuikSCAT (not wind stress as in Figure 6); blue indicates weakened or reversed wind. Contours: PGF anomaly (negative of the gradient of SLP anomaly from Figure 7 in the mean wind direction, divided by air density) at sea level in the direction of the mean wind velocity from NARR. Black contour: zero PGF anomaly. Number in each plot indicates time in days since the onset of wind relaxation at Pt. Conception. Because the mean wind velocity is not zero, the wind velocity anomaly may not change sign at the same location as the wind stress anomaly (Figure 6).

The second low-SLP anomaly is confined near sea level and has no expression at the 500 hPa level, unlike the SLP anomalies described in stage 1 above. The low SLP (blue in Figure 7, day −1 to 4) develops on the southeast side of the midlevel NPH extension (Figure 8, day −1 to 4). This is where the anticyclonic circulation associated with the NPH extension would advect warm desert air offshore. There is an offshore wind velocity anomaly off northern and central California in QuikSCAT and NARR during day 0 to 2 (not shown). Therefore, this second low-SLP anomaly is consistent with the warm air advection mechanism described in section 1.3.

That second low-SLP anomaly drives the wind relaxation at Pt. Conception during Stage 3. On day 2, the lowest SLP along the coast is near Pt. Arena (Figure 7, day 2), so the along-coast PGF anomaly is poleward from where the SLP anomaly is zero, in the SCB, to Pt. Arena (blue contours in Figure 9, day 2). This suggests the upwelling-favorable wind stress and velocity along the coast should be anomalously weak from the SCB to Pt. Arena, consistent with the wind stress and velocity anomalies from QuikSCAT (color shading in Figures 6 and 9, day 2). A similar argument holds for the rest of day −1 to 4. Therefore, the Pt. Conception wind relaxations appear to be caused by advection of warm desert air offshore of central California as a result of the NPH extensions in the "event cycles" described in section 1.3.

3.4. NARR Misses Important Wind Features Near the Coast

The mean wind stress from the reanalysis is quantitatively similar to the QuikSCAT wind stress only on synoptic scales and away from major capes. Within ~100 km of all 5 major capes, NARR, which does not

assimilate QuikSCAT data directly, misses important features of the coastal wind stress patterns. In the mean wind stress maps, the enhancement of wind stress to the south of each of the 5 major capes is very weak in NARR (Figure 2b) as compared to QuikSCAT (Figure 2a). In the mean, NARR has a weak wind stress maximum ~200–300 km offshore (Figure 2b), rather than the strong maximum ~50 km offshore in QuikSCAT (Figure 2a). In composite wind stress anomalies during relaxations calculated similarly to Figure 6 but using NARR instead of QuikSCAT, the wind relaxation off California is captured by NARR, but the preceding wind intensification is weaker, especially near capes, and the weakening of the wind off Oregon is very weak (<.03 Pa anomaly magnitude; not shown). The overall size of the enhanced upwelling-favorable wind area that drives the upwelling system is correct in NARR (the diffuse cyan area in Figure 2b is similar in size to Figure 2a), but the wind stress within 100 km of the coast and 200 km of the major capes, which is intensified by hydraulic control phenomena (section 1.2), is too weak in NARR by a factor of ~2. Offshore of ~100–200 km from the coast, the wind stress in NARR does compare well to QuikSCAT.

4. Discussion

4.1. What Causes the Pt. Conception Wind Relaxations?

The wind relaxations at Pt. Conception are caused by synoptic-scale, along-coast atmospheric pressure gradients (section 3.3). The SLP anomalies visible in NARR first strengthen, then weaken the along-coast pressure gradient force off Pt. Conception, which strengthens, then weakens the upwelling-favorable wind at Pt. Conception. This is consistent with the dynamical balance discussed in section 1.3, in which the along-coast pressure gradient influences the along-coast wind [*Halliwell and Allen*, 1987; *Beardsley et al*., 1987; *Dorman et al*., 2013].

The synoptic setup associated with the Pt. Conception wind relaxations is a later stage of the same synoptic "event sequence" described by *Halliwell and Allen* [1987] as leading to wind reversals and intensifications off Oregon and northern California (section 1.3). The synoptic patterns accompanying stages 1 and 2 of the wind progression (section 3.3) are similar to the 500 hPa trough and NPH ridging previously described as preceding and causing wind reversals off northern California [*Halliwell and Allen*, 1987; *Mass and Bond*, 1996]. The wind intensification in stage 2 was studied with QuikSCAT and NCEP by *Taylor et al*. [2008]. The second low SLP anomaly associated with the Pt. Conception relaxation (section 3.3) is consistent with the heat low described in previous studies as following the NPH extension, sometimes leading to coastally-trapped wind reversals off central California, and being caused by warm air advection offshore from the desert heat low in the southwestern U.S. due to the southeastern limb of the anticyclonic circulation associated with the NPH extension [*Mass and Bond*, 1996; *Nuss*, 2007].

The synoptic forcing of these Pt. Conception wind relaxations is typically weaker than in previous studies of strong wind reversals: ~2.5 hPa SLP anomalies and an ~80 m 500 hPa trough on average for the Pt. Conception relaxations (Figures 7 and 8), as compared to ~6 hPa and ~120 m for strong Oregon/northern California wind reversals [*Halliwell and Allen*, 1987; *Mass and Bond*, 1996]. The anomalies we studied are more comparable to the anomalies during weakly reversed winds off northern California: ~4.5 hPa and ~60 m [*Mass and Bond*, 1996, Figure 9]. In the events we studied, the along-coast pressure gradient does not, on average, change enough to cause actual wind reversal off Oregon or California (Figure 4). The strong and weak wind reversals studied equatorward of Pt. Arena by *Mass and Bond* [1996] and others (section 1.3) appear to be a subset of the larger class of weaker, synoptic-scale wind relaxations that affect oceanic flow at Pt. Conception.

4.2. What Sets the Cross-Coast Spatial Scale of Pt. Conception Relaxations?

The wind relaxations that affect Pt. Conception have a large (500–1000 km) offshore extent, in both individual relaxations (e.g., Figure 5d) and the composite anomalies (Figure 9, day 2). This cross-coast scale is approximately equal to the cross-coast scale of the prevailing winds prior to the relaxation (Figure 1) and much larger than the internal Rossby radius in the atmosphere along California, ~150 km [*Halliwell and Allen*, 1987]. However, the spatial pattern of the relaxation (Figure 6, day 2) is very similar to the expansion fan due to the large-scale bend of California [*Edwards et al*., 2002, Figure 7], both patterns widening equatorward and covering the same along-coast and cross-coast extent. This suggests that the synoptic pressure anomalies turn off the prevailing winds over the entire California-scale expansion fan, which extends

~600 km offshore (section 1.2) [*Edwards et al*., 2002]. As a result, the cross-coast scale of the relaxations is the same as that of the prevailing winds.

4.3. What Stops the Pt. Conception Relaxations From Extending Farther Poleward?

The wind relaxations that affect Pt. Conception appear to be halted near Cape Mendocino by an opposing synoptic-scale pressure gradient force anomaly. Near the coast on day 1–3 of the wind relaxation that affects Pt. Conception, the along-coast wind velocity anomaly (Figure 9, blue shading) changes sign where the along-coast pressure gradient force anomaly changes sign from poleward to equatorward (black contour). North of the region of wind relaxation, the synoptic-scale PGFa is equatorward (e.g., red in Figure 9, day 0). Therefore, the composite mean wind relaxation and the individual events (not shown) are consistent with an arrest mechanism described previously for wind reversals (section 1.3) [*Rahn and Parish*, 2010]: a synoptic-scale equatorward PGF stops the poleward extension of the wind relaxations that affect Pt. Conception and central California.

Rahn and Parish [2010] showed using a numerical model and aircraft data that as an NPH extension (e.g., section 1.3) recedes, the equatorward PGF along California is enhanced in the vicinity of Cape Mendocino due to topographic blocking of the equatorward wind creating a disturbance in the pressure field. We hypothesize that enhancement of the equatorward PGFa (red in Figure 9) by Cape Mendocino is also the reason that the zero crossing in the PGF anomaly in our Figure 9 stops moving poleward at Cape Mendocino (day 2–5) and the wind relaxation events studied here tend to terminate at the Cape. Testing this hypothesis would best be done with a higher-resolution model than NARR and is beyond the scope of this study.

4.4. Accuracy of the Wind and Pressure Fields From NARR

The wind stress in the reanalysis NARR is too weak by a factor of ~2 near the 5 major capes (section 3.5), consistent with a previous comparison of QuikSCAT to the NCEP Eta Model [*Perlin et al*., 2004]. In contrast, QuikSCAT captures the areas of intensified wind stress due to the hydraulic expansion fans at capes even though the effective resolution of QuikSCAT (~40 km) is coarser than NARR. This is because QuikSCAT records ocean surface stress, i.e., microwave radiation backscattered from capillary waves (section 2.1), regardless of the dynamics that generate that stress.

Still, the pressure field in NARR should be reliable on synoptic scales, away from major capes. Synoptic pressure variations typically occur on spatial scales greater than the grid scale of NARR (32 km), and NARR assimilates in-situ atmospheric pressure data. As a result, the synoptic-scale PGF calculated from NARR should contain useful information about what stops the poleward extension of the wind stress anomalies during Pt. Conception wind relaxations (section 4.3). This is consistent with previous studies that used National Weather Service pressure products to diagnose the relation of alongshore winds to synoptic events [*Halliwell and Allen*, 1987] or used NARR to initialize higher-resolution models.

5. Summary

This work was motivated by warm oceanic poleward flows that occur near Pt. Conception in summer [*Washburn et al*., 2011]. Those poleward oceanic flows are caused by wind relaxations detectable at Pt. Conception buoys. The wind weakens to near zero but typically does not reverse direction to downwelling-favorable (Figure 3). These relaxation events are not well-studied in the atmospheric literature compared to wind reversals farther north in the upwelling system. A previous study of the Pt. Conception wind relaxations [*Melton et al*., 2009] did not address what causes the wind relaxations or describe the offshore spatial extent of the relaxations. We used QuikSCAT satellite vector wind data to provide a regional picture of the wind relaxations at Pt. Conception, paired with reanalysis products to determine what synoptic atmospheric patterns precede and accompany the relaxation events.

Satellite wind stress anomalies on the 12 days surrounding a wind relaxation at Pt. Conception, at the border between central and southern California, composited over ~70 relaxation events during May–August 2000–2009, show 3 distinct stages of wind anomalies (Figures 4 and 6). Only the third stage is the wind relaxation at Pt. Conception. The stages are: (1) weakening or reversal of the upwelling-favorable wind in the poleward part of the California Current upwelling system, i.e., off Oregon and northern California; (2) wind intensification, in which the upwelling-favorable wind stress is stronger than the mean over much of

the upwelling system, beginning in the equatorward and progressing to the poleward part of the system; and (3) wind relaxation at Pt. Conception in the equatorward part of the upwelling system, beginning near San Diego in southern California and extending poleward through central California over ~2–3 days. The maximum extent of the weakened winds during the Pt. Conception wind relaxation, stage 3, occurs ~2 days after the Pt. Conception wind relaxation begins and ranges from Pt. Arena to Punta Eugenia in Baja California. The Pt. Conception wind relaxations are separate events from wind relaxations and reversals previously studied off Oregon [e.g., *Bane et al*., 2007], but are weaker versions of wind reversal events previously studied south of Cape Mendocino, off central California [e.g., *Halliwell and Allen*, 1987].

The wind relaxations at Pt. Conception are caused by a later stage of a known synoptic pattern. These "event cycles" typically cause weakening, and sometimes reversal, of the upwelling-favorable wind off Oregon or northern California, and then wind intensification [*Halliwell and Allen*, 1987]. The wind intensification is due to an NPH extension that advects warm air offshore from the desert heat low [*Nuss et al*., 2000] (Figures 7 and 8). The warm air advection causes a low pressure area offshore of central California, affecting the along-coast pressure gradient (Figure 9). This leads to the wind relaxation off Pt. Conception and central California, typically 5–6 days after the Oregon relaxation or reversal (Figure 6).

The composite wind anomaly from 67 wind relaxations reveals that the area of weakened winds off Pt. Conception extends 500–1000 km offshore, much farther than the wind relaxations in previous studies off northern California. The wind weakens over an area of the ocean approximately the size of California (Figure 6, day 2). The cross-coast extent of the weakened winds off central California is similar to the extent of the California-scale expansion fan characteristic of the prevailing winds [*Edwards et al*., 2002]. Therefore, wind relaxations that affect Pt. Conception involve a synoptic-scale shutdown of the prevailing upwelling-favorable winds, not a narrow band of wind anomalies along the coast such as is characteristic of coastally-trapped wind reversals. The along-coast extent of the wind relaxation appears to be determined by the synoptic-scale pressure gradient anomalies (Figure 9), which extend on average to Cape Mendocino, perhaps due to modification of the pressure field by the Cape.

Wind relaxations or reversals and associated poleward oceanic flows of warm water are important characteristics of highly-productive coastal upwelling systems worldwide. This study presents a regional-scale understanding of wind relaxation near Pt. Conception, California. The QuikSCAT satellite allowed us to discover the large offshore extent of the wind relaxations that affect the Pt. Conception area, and to link the Pt. Conception events to wind events farther poleward in the California Current upwelling system. We used coastal buoy data to form an index of events that are interesting for oceanographic or meteorological reasons, then paired that index with satellite images and reanalysis products to gain a regional-scale understanding of what forces these wind events. This strategy should be useful for studying wind relaxation in other eastern boundary upwelling systems and for studying other types of wind events.

Acknowledgments

This study was supported by NASA Ocean Vector Winds Science Team Grants NNX10AO94G to UCSB and NNX14AI06G to UConn, and National Science Foundation grants OCE-0957948 and OCE-1031893. We are grateful to P. Ted Strub, Dudley Chelton, Craig Risien, Barry Vanhoff, and Corinne James (OSU); David Long (BYU); Ralph Milliff (U. Colorado); Ad Stoffelen and Tilly Driesenaar (KNMI); Mark Bourassa (FSU); Deborah Smith (Remote Sensing Systems); and David Moroni, W. Timothy Liu, and Bryan Stiles (NASA/JPL) for advice on selecting a QuikSCAT data product and the correct use of swath data. Brian Emery was very helpful in accessing and processing the NARR output. We thank James Edson (UConn) for helpful discussions. Meghan F. Cronin (NOAA) provided helpful writing suggestions. For some plots we used M_MAP by Rich Pawlowicz and JLAB: Lilly, J. M. (2012), JLAB: Matlab freeware for data analysis, Version 0.94, http://www.jmlilly.net/software.html. Carlos Moffat (U. Delaware) provided Matlab code and helpful comments on an earlier version of the manuscript. We thank $n \geq 2$ anonymous reviewers and John Bane (UNC Chapel Hill) for helping us improve the manuscript. All the QuikSCAT, NARR, and buoy data are available online (section 2.1).

References

Bane, J. M., M. D. Levine, R. M. Samelson, S. M. Haines, M. F. Meaux, N. Perlin, P. M. Kosro, and T. Boyd (2005), Atmospheric forcing of the Oregon Coastal Ocean during the 2001 upwelling season, *J. Geophys. Res.*, *110*, C10S02, doi:10.1029/2004JC002653.

Bane, J. M., Y. H. Spitz, R. M. Letelier, and W. T. Peterson (2007), Jet stream intraseasonal oscillations drive dominant ecosystem variations in Oregon's summertime coastal upwelling system, *Proc. Natl. Acad. Sci. U. S. A.*, *104*(33), 13,262–13,267, doi:10.1073/pnas.0700926104.

Beardsley, R. C., C. E. Dorman, C. A. Friehe, L. K. Rosenfeld, and C. D. Winant (1987), Local atmospheric forcing during the Coastal Ocean Dynamics Experiment 1: A description of the marine boundary layer and atmospheric conditions over a northern California upwelling region, *J. Geophys. Res.*, *92*, 1467–1488, doi:10.1029/JC092iC02p01467.

Blanchette, C. A, C. M. Miner, P. T. Raimondi, D. Lohse, K. E. K. Heady, and B. R. Broitman (2008), Biogeo graphical Patterns of Rocky Intertidal Communities Along the Pacific Coast of North America, *J. Biogeography*, *35*(9), 1593–1607, doi:10.1111/j.1365-2699.2008.01913.x.

Bond, N. A., C. F. Mass, and J. E. Overland (1996), Coastally trapped wind reversals along the united states west coast during the warm season. Part I: Climatology and temporal evolution, *Mon. Weather Rev.*, *124*(3), 430–445, doi:10.1175/1520-0493(1996)124 < 0430:CTWRAT>2.0.CO;2.

Bosart, L. (1983), Analysis of a California Catalina eddy event, *Mon. Wea. Rev.*, *111*(8), 1619–1633.

Chan, F., J. A. Barth, J. Lubchenco, A. Kirincich, H. Weeks, W. T. Peterson, and B. A. Menge (2008), Emergence of anoxia in the California Current large marine ecosystem, *Science*, *319*, 920, doi:10.1126/science.1149016.

Chelton, D., A. Bratkovich, R. Bernstein, and P. Kosro (1988), Poleward flow off central California during the spring and summer of 1981 and 1984, *J. Geophys. Res.*, *93*(C9), 10,604–10,620, doi:10.1029/JC093iC09p10604.

Cudaback, C. N., L. Washburn, and E. Dever (2005), Subtidal inner-shelf circulation near Point Conception, California, *J. Geophys. Res.*, *110*, C10007, doi:10.1029/2004JC002608.

Dever, E. P. (2004), Objective maps of near-surface flow states near Point Conception, California, *J. Phys. Oceanogr.*, *34*, 444–461.

Dever, E., M. Hendershott, and C. Winant (1998), Statistical aspects of surface drifter observations of circulation in the Santa Barbara Channel, *J. Geophys. Res.*, *103*(C11), 24,781–24,797, doi:10.1029/98JC02403.

Dorman, C. E., and D. Koračin (2008), Response of the summer marine layer flow to an extreme California Coastal Bend, *Mon. Weather Rev.*, *136*, 2894–2922, doi:10.1175/2007MWR2336.1.
Dorman, C. E, and C. D. Winant (1995), Buoy Observations of the Atmosphere Along the West Coast of the United States, 1981–1990, *J. Geophys. Res.*, *100*, 16,029–16,044, doi:10.1029/95JC00964.
Dorman, C. E., and C. D. Winant (2000), The structure and variability of the marine atmosphere around the Santa Barbara Channel, *Mon. Weather Rev.*, *128*(2), 261–282, doi:10.1175/1520-0493(2000)128%3C0261:TSAVOT%3E2.0.CO;2.
Dorman, C. E., D. P. Rogers, W. Nuss, and W. T. Thompson (1999), Adjustment of the summer marine boundary layer around Pt. Sur, California, *Mon. Weather Rev.*, *127*, 2143–2159, doi:10.1175/1520-0493(1999)127%3C2143:AOTSMB%3E2.0.CO;2.
Dorman, C. E., T. Holt, D. P. Rogers, and K. Edwards (2000), Large-Scale Structure of the June–July 1996 Marine Boundary Layer Along California and Oregon, *Mon. Weather Rev.*, *128*, 1632–1652, doi:10.1175/1520-0493(2000)128%3C1632:LSSOTJ%3E2.0.CO%3B2.
Dorman, C. E., E. P. Dever, and J. Largier (2006), Buoy Measured Wind, Wind Stress and Curl of the Wind Stress Over the Shelf off Bodega Bay, California, *Deep Sea Res., Part II*, *53*, 2850–2864, doi:10.1016/j.dsr2.2006.07.006.
Dorman, C. E., Mejia, J. F., and D. Koračin (2013), Impact of US West Coastline Inhomogeneity and Synoptic Forcing on Winds, Wind Stress, and Wind Stress Curl During Upwelling Season, *J. Geophys. Res. Oceans*, *118*, 4036–4051, doi:10.1002/jgrc.20282.
Dudas, S. E., B. A. Grantham, A. R. Kirincich, B. A. Menge, J. Lubchenco, and J. A. Barth (2009), Current reversals as determinants of intertidal recruitment on the central Oregon coast, *ICES J. Mar. Sci.*, *66*, 396–407, doi:10.1093/icesjms/fsn179.
Edson, J., V. Jampana, R. Weller, S. Bigorre, A. Plueddemann, C. Fairall, S. Miller, L. Mahrt, D. Vickers, and H. Hersbach (2013), On the exchange of momentum over the open ocean, *J. Phys. Oceanogr.*, *43*, 1589–1610, doi:10.1175/JPO-D-12-0173.1.
Edwards, K. A. (2000), The marine atmospheric boundary layer during Coastal Waves 96, PhD thesis, Univ. of Calif., San Diego, San Diego.
Edwards, K. A., A. M. Rogerson, C. D. Winant, and D. P. Rogers (2001), Adjustment of the marine atmospheric boundary layer to a coastal cape, *J. Atmos. Sci.*, *58*, 1511–1528, doi:10.1175/1520-0469(2001)058 < 1511:AOTMAB>2.0.CO;2.
Edwards, K. A., D. P. Rogers, and C. E. Dorman (2002), Adjustment of the marine atmospheric boundary layer to the large-scale bend in the California coast, *J. Geophys. Res.*, *107*(C12), 3213, doi:10.1029/2001JC000807.
Enriquez, A. G., and C. A. Friehe (1995), Effects of wind stress and wind stress curl variability on coastal upwelling, *J. Phys. Oceanogr.*, *25*, 1651–1671, doi:10.1175/1520-0485(1995)025 < 1651:EOWSAW>2.0.CO;2.
Fawcett, A. L., G. C. Pitcher, and F. A. Shillington (2008), Nearshore currents on the southern Namaqua shelf of the Benguela upwelling system, *Cont. Shelf Res.*, *28*(8), 1026–1039, doi:10.1016/j.csr.2008.02.005.
Fore, A. G., B. W. Stiles, A. H. Chau, B. A. Williams, R. S. Dunbar, and E. Rodriguez (2014), Point-wise wind retrieval and ambiguity removal improvements for the QuikSCAT climatological data set, *IEEE Trans. Geosci. Remote Sens.*, *52*(1), 5159, doi:10.1109/TGRS.2012.2235843.
Gan, J., and J. S. Allen (2002a), A modeling study of shelf circulation off northern California in the region of the Coastal Ocean Dynamics Experiment: Response to relaxation of upwelling winds, *J. Geophys. Res.*, *107*(C9), 3123, doi:10.1029/2000JC000768.
Gan, J., and J. S. Allen (2002b), A modeling study of shelf circulation off northern California in the region of the Coastal Ocean Dynamics Experiment, 2, Simulations and comparisons with observations, *J. Geophys. Res.*, *107*(C11), 3184, doi:10.1029/2001JC001190.
García-Lafuente, J., J. Delgado, F. Criado-Aldeanueva, M. Bruno, J. del Rio, and J. M. Vargas (2006), Water mass circulation on the continental shelf of the Gulf of Cádiz, *Deep Sea Res., Part II*, *53*, 1182–1197, doi:10.1016/j. dsr2.2006.04.011.
Garel, E., I. Laiz, T. Drago, and P. Relvas (2016), Characterisation of coastal counter-currents on the inner shelf of the Gulf of Cadiz, *J. Mar. Syst.*,*155*, 19–34, doi:10.1016/j.jmarsys.2015.11.001.
Grantham, B. A, F. Chan, K. J. Nielsen, D. S. Fox, J. A. Barth, A. Huyer, J. Lubchenco, and B. A Menge (2004), Upwelling-driven nearshore hypoxia signals ecosystem and oceanographic changes in the Northeast Pacific, *Nature*, *429*, 749–754, doi:10.1038/nature02605.
Halliwell, G. R., and J. S. Allen (1987), The large-scale coastal wind field along the west coast of North America, 1981–1982, *J. Geophys. Res.*, *92*, 1861–1884, doi:10.1029/JC092iC02p01861.
Harms, S., and C. Winant (1998), Characteristic patterns of the circulation in the Santa Barbara Channel, *J. Geophys. Res.*, *103*(C2), 3041–3065, doi:10.1029/97JC02393.
Hickey, B. M. (1979), The California Current System—Hypotheses and facts, *Prog. Oceanogr.*, *8*(4), 191–279, doi:10.1016/0079-6611(79)90002-8.
Hu, H., and T. Liu (2002), QuikSCAT reveals the surface circulation of the Catalina Eddy, *Geophys. Res. Lett.*, *29*(17), 1821, doi:10.1029/2001GL014203.
Koračin, D., C. E. Dorman, and E. P. Dever (2004), Coastal Perturbations of Marine Layer Winds, Wind Stress, and Wind Stress Curl Along California and Baja California in June 1999, *J. Phys. Oceanogr.*, *34*, 1152–1173, doi:10.1175/1520-0485(2004)034%3C1152:CPOMWW%3E2.0.CO%3B2.
Largier, J. L., B. A. Magnell, and C. D. Winant (1993), Subtidal circulation over the northern California shelf, *J. Geophys. Res.*, *98*(C10), 18,147–18,179, doi:10.1029/93JC01074.
Lentz, S. (1987), A heat budget for the northern California shelf during CODE 2, *J. Geophys. Res.*, *92*(C13), 14,491–14,509.
Lynn, R, J, and J. J. Simpson (1987), The California Current System: The seasonal variability of its physical characteristics, *J. Geophys. Res.*, *92*, 12,947–12,966, doi:10.1029/JC092iC12p12947.
Mace, A. J., and S. G. Morgan (2006a), Biological and physical coupling in the lee of a small headland: Contrasting transport mechanisms for crab larvae in an upwelling region, *Mar. Ecol. Prog. Ser.*, *324*, 185–196, doi:10.3354/meps324185.
Mace, A. J., and S. G. Morgan (2006b), Larval accumulation in the lee of a small headland: Implications for the design of marine reserves, *Mar. Ecol. Prog. Ser.*, *318*, 19–29, doi:10.3354/meps318019.
Mass, C. F., and M. D. Albright (1989), Origin of the Catalina Eddy, *Mon. Wea. Rev.*, *117*, 2406–2436, doi:10.1175/1520-0493(1989)117<2406:OOTCE>2.0.CO;2.
Mass, C. F., and N. A. Bond (1996), Coastally trapped wind reversals along the United States West Coast during the warm season. Part II: Synoptic evolution, *Mon. Weather Rev.*, *124*(3), 446–461, doi:10.1175/1520-0493(1996)124 < 0446:CTWRAT>2.0.CO;2.
Melton, C., L. Washburn, and C. Gotschalk (2009), Wind relaxations and poleward flow events in a coastal upwelling system on the Central California Coast, *J. Geophys. Res.*, *114*, C11016, doi:10.1029/2009JC005397.
Mesinger, F., et al. (2006), North American Regional Reanalysis, *Bull. Am. Meteorol. Soc.*, *87*(3), 343–360, doi:10.1175/BAMS-87-3-343.
Neiburger, M., D. S. Johnson and C. W. Chien (1961), Studies of the structure of the atmosphere over the eastern Pacific Ocean in the summer, in *The Inversion Over the Eastern North Pacific Ocean*, pp. 1–94, Univ. of Calif. Press, Berkeley.
Nelson, C. S. (1977), Wind stress and wind stress curl over the California Current, *NOAA Tech. Rep. NMFS SSRF-714, NTIS PB-273610*, 95 pp., Natl. Oceanic and Atmos. Admin., Natl. Mar. Fish. Serv., Seattle, Wash.
Nelson, C. S., and D. M. Husby (1983), Climatology of surface heat fluxes over the California Current region, *NOAA Tech. Rep. NMFS SSRF-763, NTIS PB83-193631*, 155 pp., Natl. Oceanic and Atmos. Admin., Natl. Mar. Fish. Serv., Highlands, N. J.

Nidzieko, N. J., and J. L. Largier (2013), Inner shelf intrusions of offshore water in an upwelling system affect coastal connectivity, *Geophys. Res. Lett.*, *40*(20), 5423–5428, doi:10.1002/2013GL056756.
Nuss, W. A. (2007), Synoptic-scale structure and the character of coastally trapped wind reversals, *Mon. Weather Rev.*, *135*, 60–81, doi:10.1175/MWR3267.1.
Nuss, W. A., et al. (2000), Coastally trapped wind reversals: Progress toward understanding, *Bull. Am. Meteorol. Soc.*, *81*(4), 719–743, doi:10.1175/1520-0477(2000)081 < 0719:CTWRPT>2.3.CO;2.
Overland, J. (1984), Scale analysis of marine winds in straits and along mountainous coasts, *Mon. Weather Rev.*, *112*, 2532–2536, doi:10.1175/1520-0493(1984)112 < 2530:SAOMWI>2.0.CO;2.
Parish, T. R., D. A. Rahn, and D. Leon (2008), Aircraft observations of a coastally trapped wind reversal off the California coast, *Mon. Weather Rev.*, *136*, 644–662, doi:10.1175/2007MWR2199.1.
Pauly, D., and V. Christensen (1995), Primary production required to sustain global fisheries, *Nature*, *374*, 255–257, doi:10.1038/374255a0.
Perlin, N., R. Samelson, and D. Chelton (2004), Scatterometer and Model Wind and Wind Stress in the Oregon–Northern California Coastal Zone, *Mon. Weather Rev.*, *132*(8), 2110–2129, doi:10.1175/1520-0493(2004)132 < 2110:SAMWAW>2.0.CO;2.
Pickett, M. H., and J. D. Paduan (2003), Ekman transport and pumping in the California Current based on the U.S. Navy's high-resolution atmospheric model (COAMPS), *J. Geophys. Res.*, *108*(C10), 3327, doi:10.1029/2003JC001902.
Rahn, D. A., and T. R. Parish (2008), A study of the forcing of the 22–25 June 2006 coastally trapped wind reversal based on numerical simulations and aircraft observations, *Mon. Weather Rev.*, *136*, 4687–4708, doi:10.1175/2008MWR2361.1.
Rahn, D. A, and T. R. Parish (2010), Cessation of the 22–25 June 2006 coastally trapped wind reversal, *J. Appl. Meteorol. Climatol.*, *49*(7), 1412–1428, doi:10.1175/2010JAMC2242.1.
Ralph, F. M., L. Armi, J. M. Bane, C. Dorman, W. D. Neff, P. J. Neiman, W. Nuss, and P. O. G. Persson (1998), Observations and analysis of the 10-11 June 1994 coastally trapped disturbance, *Mon. Weather Rev.*, *126*, 2435–2465, doi:10.1175/1520-0493(1998)126 < 2435:OAAOTJ>2.0.CO;2.
Relvas, P., and E. D. Barton (2002), Mesoscale patterns in the Cape São Vicente (Iberian Peninsula) upwelling region, *J. Geophys. Res.*, *107*(C10), 3164, doi:10.1029/2000JC000456.
Relvas, P., and E. D. Barton (2005), A separated jet and coastal counter-flow during upwelling relaxation off Cape São Vicente (Iberian Peninsula), *Cont. Shelf Res.*, *25*, 29–49, doi:10.1016/j.csr.2004.09.006.
Ricciardulli, L., and F. Wentz (2011), Reprocessed QuikSCAT (V04) wind vectors with Ku-2011 geophysical model function, *Tech. Rep. 043011*, Remote Sens. Syst., Santa Rosa, Calif. [Available at http://www.ssmi.com/qscat/qscat_Ku2011_tech_report.pdf.]
Rogers, D., et al. (1998), Highlights of coastal waves 1996, *Bull. Am. Meteorol. Soc.*, *79*, 1307–1326, doi:10.1175/1520-0477(1998)079 < 1307:HOCW>2.0.CO;2.
Rogerson, A. M. (1999), Transcritical flows in the coastal marine atmospheric boundary layer, *J. Atmos. Sci.*, *56*, 2761–2779, doi:10.1175/1520-0469(1999)056%3C2761:TFITCM%3E2.0.CO;2.
Samelson, R. M. (1992), Supercritical marine layer flow along a smoothly varying coastline, *J. Atmos. Sci.*, *49*, 1571–1584, doi:10.1175/1520-0469(1992)049%3C1571:SMLFAA%3E2.0.CO%3.
Send, U., R. C. Beardsley, and C. D. Winant (1987), Relaxation from upwelling in the Coastal Ocean Dynamics Experiment, *J. Geophys. Res.*, *92*, 1683–1698, doi:10.1029/JC092iC02p01683.
Skamarock, W. C., R. Rotunno, and J. B. Klemp (2002), Catalina eddies and coastally trapped disturbances, *J. Atm. Sci.*, *59*, 2270–2278.
Taylor, S. V., D. R. Cayan, N. E. Graham, and K. P. Georgakakos (2008), Northerly surface winds over the eastern North Pacific Ocean in Spring and Summer, *J. Geophys. Res.*, *113*, D02110, doi:10.1029/2006JD008053.
U.S. Navy (1956), Marine climatic atlas of the World, vol. II, North Pacific Ocean, *Rep. NAVAER 50-1C-529*, 275 pp., U.S. Gov. Print. Off., Washington, D. C.
Washburn, L., M. R. Fewings, C. Melton, and C. Gotschalk (2011), The propagating response of coastal circulation due to wind relaxations along the Central California Coast, *J. Geophys. Res.*, *116*, C12028, doi:10.1029/2011JC007502.
Wilson, J. R., B. R. Broitman, J. E. Caselle, and D. E. Wendt (2008), Recruitment of coastal fishes and oceanographic variability in central California, *Estuar. Coast. Shelf Sci.*, *79*(3), 483–490, doi:10.1016/j.ecss.2008.05.001.
Winant, C., E. Dever, and M. Hendershott (2003), Characteristic patterns of shelf circulation at the boundary between central and southern California, *J. Geophys. Res.*, *108*(C2), 3021, doi:10.1029/2001JC001302.
Winant, C. D., C. E. Dorman, C. A. Friehe, and R. C. Beardsley (1988), The marine layer off northern California: An example of supercritical channel flow, *J. Atmos. Sci.*, *45*, 3588–3605, doi:10.1175/1520-0469(1988)045 < 3588:TMLONC>2.0.CO;2.
Wing, S. R., L. W. Botsford, J. L. Largier, and L. E. Morgan (1995a), Spatial structure of relaxation events and crab settlement in the northern California upwelling system, *Mar. Ecol. Prog. Ser.*, *128*, 199–211, doi:10.3354/meps128199.
Wing, S., J. Largier, L. Botsford, and J. Quinn (1995b), Settlement and transport of benthic invertebrates in an intermittent upwelling region, *Limnol. and Oceanogr.*, *40*(2), 316–329, doi:10.4319/lo.1995.40.2.0316.
Woodson, C. B., L. Washburn, J. A. Barth, D. J. Hoover, A. R. Kirincich, M. A. McManus, J. P. Ryan, and J. Tyburczy (2009), Northern Monterey Bay upwelling shadow front: Observations of a coastally and surface-trapped buoyant plume, *J. Geophys. Res.*, *114*, C12013, doi:10.1029/2009JC005623.
Zemba, J., and C. A. Friehe (1987), The marine atmospheric boundary layer jet in the Coastal Ocean Dynamics Experiment, *J. Geophys. Res.*, *92*, 1489–1496, doi:10.1029/JC092iC02p01489.